

Sea-level, storms, and sedimentation – Controls on the architecture of the Andros tidal flats (Great Bahama Bank)

Mingyue Wu, Paul (Mitch) Harris, Gregor Eberli, Sam J. Purkis *

CSL – Center for Carbonate Research, Department of Marine Geosciences, Rosenstiel School of Marine and Atmospheric Science, University of Miami, Miami, FL 33149, USA

ARTICLE INFO

Article history:

Received 9 March 2021

Received in revised form 26 April 2021

Accepted 27 April 2021

Available online 6 May 2021

Editor: Dr. Brian Jones

Keywords:

Andros Island

Bahamas

Carbonate tidal flats

Remote sensing

ABSTRACT

Integrated time-separated remote sensing, geographic information systems (GIS), microbiology, and carbonate sedimentology of the tidal-flat portion of Andros Island (Great Bahama Bank) quantify the geomorphologic change of tidal-flat facies through time and illustrate how sea-level rise, among other controls, is recorded within these deposits. In the 75 years spanned by the remote-sensing datasets, sea level has risen by approximately 10 cm. In the face of this change: a) the seaward margin of the tidal flats has remained static, while b) the internal boundary, which separates the channelized and supratidal marsh deposits, retrograded up to 220 m, broadening the channelized zone, and c) in unison to the broadening of the channelized zone, the abundance of laminated (*Scytonema*) cyanobacterial fabrics decreased, d) accompanied by the lengthening and avulsion of the network of tidal channels that traverse this zone. Given the amount of sea level rise during the period of observation, such broad-scale restructuring of the Andros tidal-flat architecture is surprising. The muddy tidal flats did not prograde, but instead aggraded and locally retrograded. Whereas retrogradation was minimal at the coastline, the channelized zone retrograded substantially over the more landward supratidal inland marsh. These results question aspects of the autocyclic model for the development of peritidal carbonate cycles, which is underpinned by a dominant behavior of tidal-flat progradation. Whereas other controls cannot be explicitly excluded, sea-level oscillations seemingly exerted considerably more impact on the Andros tidal flat in the last decades than did major storm events.

© 2021 Elsevier B.V. All rights reserved.

1. Introduction

Laterally-extensive accumulations of carbonate mud occur along the western edge of Andros Island on Great Bahama Bank (GBB) (Fig. 1A, B). The muddy tidal-flat complex is up to 16 km wide and extending 120 km in a north–south direction and mantles the western margin of Andros Island (Shinn et al., 1969; Hardie, 1977; Maloof and Grotzinger, 2012). As shown by these workers, the tidal flat is a wedge of modern sediments (Fig. 1C) with a typical thickness of 1.0 and 2.0 m and an accumulation rate of 1.5 to 2.0 mm year⁻¹ averaged over the full thickness of the Holocene stratigraphy. The tidal-flat complex formed from muds originating across the interior of GBB, which have been transported eastwards by tides and storms, to accumulate in the protected lee of Andros Island.

The Andros tidal flats are composed of a complex suite of sub-environments (Fig. 1B). The flats are often characterized by dendritic networks of tidal channels which partially incise the substantial Holocene lime-mud wedge, as well as the more expansive, mat-covered supratidal zone further landward. In Wu (2020) and herein, the

schemes proposed by Shinn et al. (1969) and Hardie (1977) that partition the Andros tidal-flat into three shore-parallel regions are slightly modified: (1) the subtidal platform interior; (2) the channelized zone (or ‘belt’ of Shinn et al., 1969), and (3) the supratidal inland *Scytonema* marsh that is the largest area of the tidal-flat complex (Fig. 1B, C). The latter zone is named by virtue of the extensive colonization by *Scytonema*, a genus of multicellular, filamentous cyanobacteria which forms sediment-binding mats. The presence of *Scytonema* mats is not restricted to the inland marsh; laterally discontinuous, discrete patches of *Scytonema* also inhabit slightly elevated portions [supratidal] adjacent to channel levees within the channelized zone. Because of their dark color, these patches are easily resolved in remote sensing data (e.g., in Blue Creek, Fig. 2A, B). The channels within the channelized zone commonly have mud-covered bottoms, often stabilized by seagrass, but locally shelly/intraclast lags or exposed Pleistocene limestone occurs. The channel levees and inland marsh are characterized by interlaminated mud and sand-sized pellets, whereas ponds within the channelized zone contain bioturbated, fossiliferous mud. The pond muds differ from the burrowed, pelleted mud that occurs in the subtidal platform interior immediately offshore of the tidal flats in having a less diverse biota and a distinctive brown color, as opposed to the reduced gray color of offshore muds. Blocks of cyanobacteria-coated, cohesive

* Corresponding author.

E-mail address: spurkis@rsmas.miami.edu (S.J. Purkis).

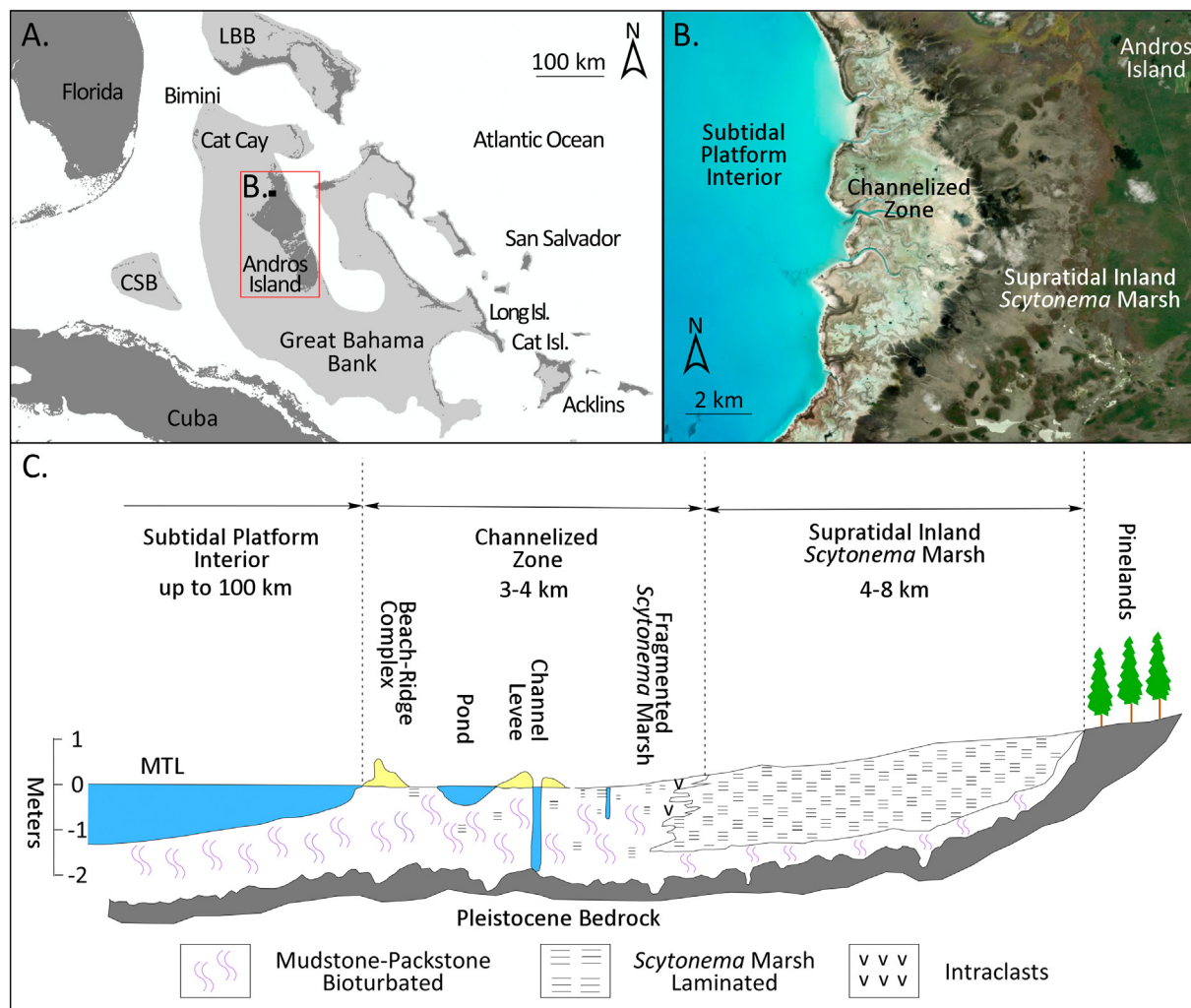


Fig. 1. (A) The Great Bahama Bank (GBB) is the largest modern isolated carbonate platform on Earth and situated at the southern extremity of North America's eastern continental margin. CSB = Cay Sal Bank; LBB = Little Bahama Bank; TOTO = Tongue of the Ocean. Gray-shading indicates water depth <20 m. Andros Island in the red box, the largest island atop GBB, is located along a windward margin of the platform. Black box on the west coast of Andros Island shows the location of a section of the tidal flats shown in the satellite image (B) which can be divided into three distinct facies belts, from offshore to onshore; the subtidal platform interior, the channelized zone, and the supratidal inland *Scytonema* marsh. (C) Schematic cross-section across (dip-oriented, from subtidal to the west to supratidal to the east) modified from Hardie (1977) showing the three zones developed in (B). (For interpretation of the references to color in this figure legend, the reader is referred to the web version of this article.)

mud are reworked from the levees as they are undercut by the channel. The crests of the levees are mud cracked, with the cracks being smaller and shallower than those typifying the microbial mat on the supratidal inland marsh (Hardie, 1977).

As emphasized in previous studies (Shinn et al., 1969; Hardie, 1977; Rankey, 2002), since the Andros tidal flats span shallow subtidal, intertidal, and supratidal zones, their architecture is sensitive to sea-level change, among a host of other controls. Perplexing problems confronting sedimentologists are an understanding of tidal-flat evolution, the relative importance of tidal flats in the stratigraphic record, and petrophysical attributes which permit these 'low-energy' sediments to develop into potential seals and/or hydrocarbon reservoirs (Roehl, 1967; Fagherazzi et al., 2006; Maloof and Grotzinger, 2012; Jahnert and Collins, 2013). Since the late 1960s, studies have extensively assessed the stratigraphy of both modern and ancient carbonate tidal flats and provided insights into their depositional patterns and lithologic attributes (Shinn et al., 1965; Laporte, 1967; Roehl, 1967; Shinn et al., 1969; Hardie, 1977; Rankey, 2002; Rankey and Morgan, 2002; Rankey et al., 2004; Maloof and Grotzinger, 2012). For example, Shinn et al. (1965) recognized that penecontemporaneous or early-diagenetic dolomite occurs on the Andros tidal flats, and Shinn et al.

(1969) described the sub-environments and facies of the Andros tidal-flat complex, including their distribution, sedimentary structures, sediments, and living fauna. The Holocene sediment record of the tidal flats is generally of bioturbated, unlaminated, pelleted mud and silt (Shinn et al., 1965; Hardie and Ginsburg, 1977). Layered sediment exists only as a thin cap over bioturbated sediment in the levees which locally form along channels in the channelled zone, and as thin-bedded inland marsh sediment (Fig. 1C). Homogenization of layered sediment by marine organisms is a major sedimentary process on subtidal and intertidal parts of the tidal flats, and layering is preserved only where burrowing organisms are excluded by prolonged subaerial exposure (Hardie and Ginsburg, 1977).

The evolution of the Andros tidal flats has been used as an analog for the architecture of carbonate peritidal cycles present in the rock record. An autocyclic model for regressive carbonate cycles, based on the Andros tidal flat, was proposed by Ginsburg (1971). He postulated that sediment transported from the offshore marine would force the tidal-flat shoreline to prograde seaward across the shallow, relatively flat top of GBB, thereby reducing the productive mud-producing area. Progradation would cease once the reduced production of mud no longer exceeded the slow, continuous subsidence of the platform.

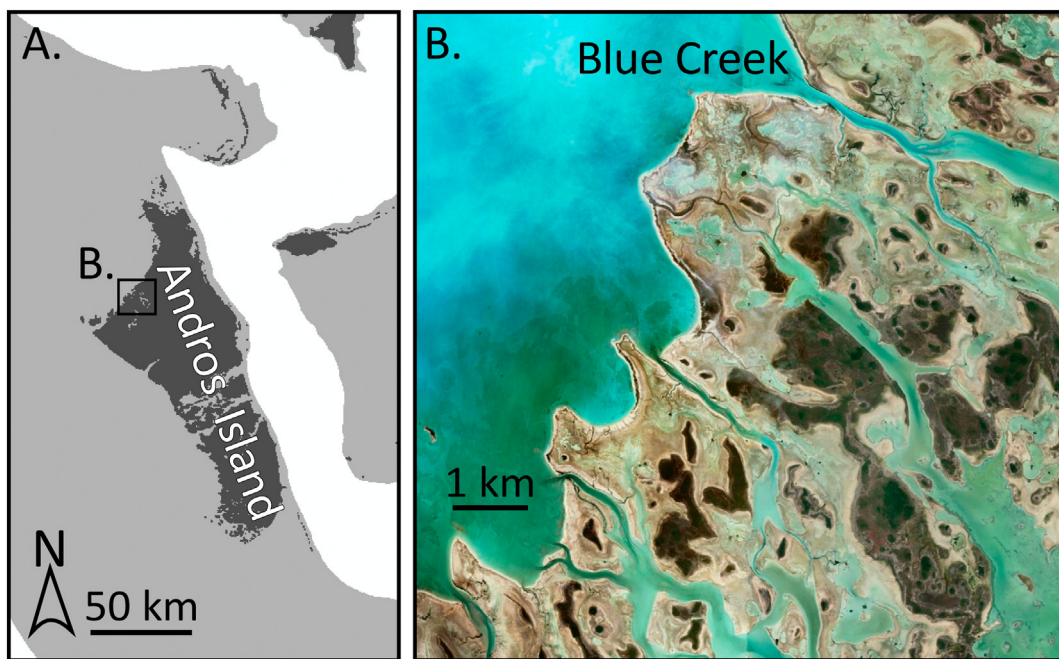


Fig. 2. The Blue Creek region of the Andros tidal flats, located by the black box in A and imaged from satellite in B, emphasizes local colonization by *Scytonema*. This genus of multicellular filamentous cyanobacteria forms laterally continuous mats which, due to their dark color, are easily resolved from true-color satellite imagery – small ovoid to irregular-shaped darkest patches in (B). (For interpretation of the references to color in this figure legend, the reader is referred to the web version of this article.)

Following a period of subsidence and a flooding of the tidal flats, the scenario would repeat. [Maloof and Grotzinger \(2012\)](#) reconstructed the Holocene evolution of the Andros tidal flats based upon facies distribution from extensive coring. The authors invoked both allogeic (e.g., sea level) and autogenic forcing mechanisms (e.g., migrating channels) for the development of the modern tidal-flat facies mosaic. The [Ginsburg \(1971\)](#) model does not incorporate storms as a possible influence on tidal-flat architecture and sediment distribution, despite the fact that Andros Island is subjected to frequent hurricanes. The [Maloof and Grotzinger \(2012\)](#) model, meanwhile, recognizes storms as a cause of landward transport of sediments across the flats, but does not posit that they exert meaningful sway over the broad-scale architecture of the Holocene deposits. In contrast, as demonstrated by [Ball et al. \(1967\)](#) for Hurricane Donna in South Florida, storms might plausibly have capacity to influence tidal-flat architecture and sediment distribution.

In this study, we build forward from past work and use time-separated remote sensing data spanning 75 years and quantitative insights that combine lateral and vertical facies dynamics, and their relationships, in order to better understand the recent evolution of the Andros tidal-flat complex. While not ruling out other controls, the overall goal of this study is to understand the sedimentological response of carbonate depositional systems to changing sea level and storm impacts. To achieve this goal, this study focuses on the channelized zone and: (i) examines the migration of the seaward and landward boundaries of the zone, (ii) reconstructs the dynamics of patterning of *Scytonema* patches, (iii) quantifies the evolution of the length of the tidal network of creeks which traverse the channelized zone, and (iv) assembles these data to predict how sea-level rise might be recorded in the rock record of a tidal-flat environment. The study builds upon a growing body of literature (e.g., [Shinn et al., 1965, 1969; Hardie, 1977; Rankey and Morgan, 2002; Rankey et al., 2004; Maloof and Grotzinger, 2012](#)) which suggests that the evolution of carbonate tidal flats under icehouse conditions, as prevail today, is predominantly determined by allogeic drivers – sea level, in particular. This is in stark contrast to the radical and short-term reconfiguration of equivalent siliciclastic settings, wrought by autogenic drivers within the system ([Fagherazzi, 2008; Purkis et al., 2016](#)).

To achieve the four specific aims, the study calls upon data collected in the field in the Three Creeks area of the tidal flats, sea-level data recorded at the three most proximal research-quality tidal gauges to Andros Island (Settlement Point, Grand Bahama Island; and Virginia Key and Key West, Florida), historical storm tracks across the Bahamas, aerial photographs acquired in 1943, and a portfolio of high-resolution satellite imagery spanning 1985 through 2018 assembled in Google Earth Engine.

2. Geological and environmental setting

2.1. Geological setting

The GBB is located at the southern extremity of North America's eastern continental margin and is the largest isolated carbonate platform on Earth. GBB formed by the coalescence of smaller isolated platforms ([Eberli and Ginsburg, 1987](#)) and, as a modern location of major carbonate deposition, has fostered a fundamental understanding of many depositional processes of carbonate sedimentation. The GBB serves as a training venue for academia and industry, is the basis for numerous geological models, and is often used as a reservoir analog ([Harris et al., 2015; Purkis and Harris, 2016](#)). Andros Island, the largest island atop GBB at 5960 km² in size, is located on an east-facing margin of the western portion of the platform (red box in [Fig. 1A](#)) where it is bounded by the deep Tongue of the Ocean (TOTO) immediately to the east. On the eastern side of Andros, Pleistocene eolian ridges run parallel along the strike of the island. The western side of the island, however, is low with Holocene muds overlying a relatively flat and westerly-dipping Pleistocene surface ([Fig. 1C](#)). This mud wedge forms a shore-parallel belt 120 km long – the Andros tidal flats. To the north, the tidal flats are relatively narrow and only partly incised by tidal channels; whereas to the south, the tidal-flat belt is wider and wetter, being cut by more substantial tidal channels and hosting numerous ponds and lakes.

2.2. Environmental setting

Since the environmental setting of the Andros Island tidal flats influences their sediment dynamics, a review is warranted. The Andros

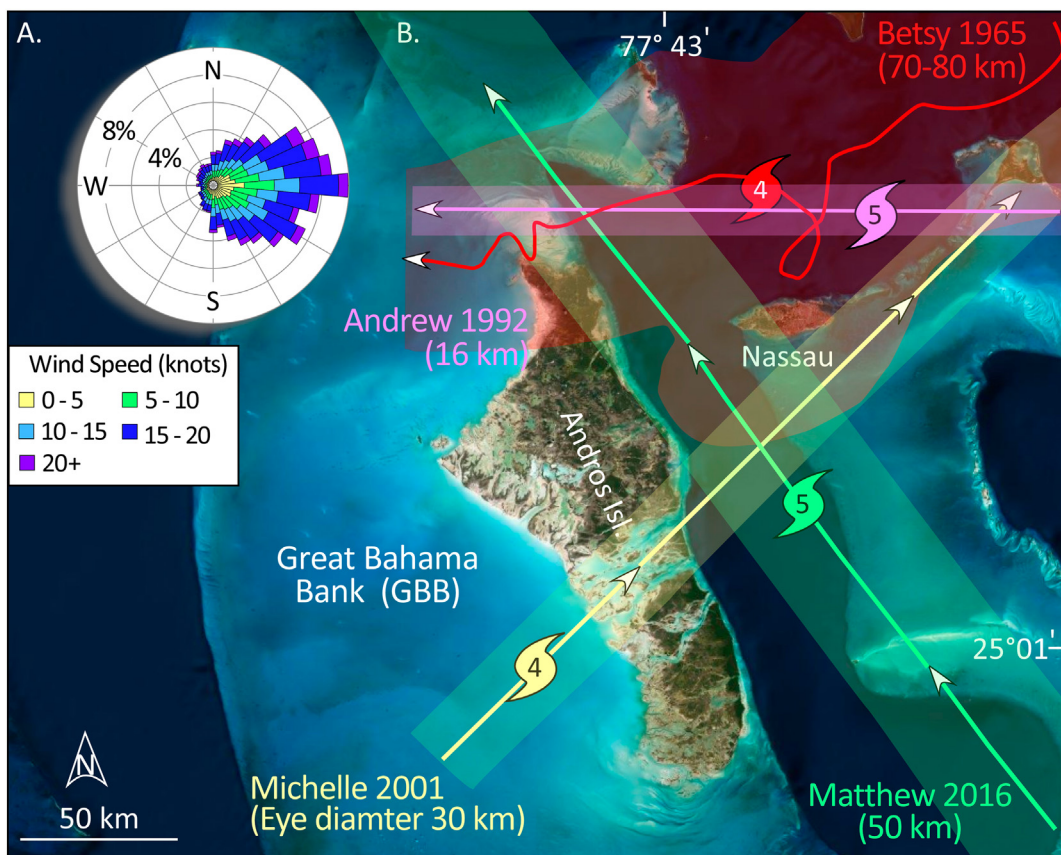


Fig. 3. (A) Shows a wind rose capturing wind speed and direction extracted from QuikSCAT satellite observations for the period January 2013 to January 2014. (B) Three major hurricanes passed in close proximity to Andros between 1985 and 2018: Hurricane Andrew (Category 5) in 1992, Michelle (Cat. 4) in 2001, and Matthew (Cat. 5) in 2016. The tracks of these three storms, plus Category 4 Betsy (1965), are plotted atop true-color satellite imagery. Colored lines represent the tracks of these storms and the diameters of their eyes is depicted either side of each track. Eye diameters are also given in units of kilometers after the storm names. Note how the diameter of the hurricane's eyes is decoupled from the strength of the storms. Michelle and Betsy were both Category 4 storms, but Betsy's eye (80 km) was more than double the breadth of Michelle's (30 km). (For interpretation of the references to color in this figure legend, the reader is referred to the web version of this article.)

climate is tropical-maritime with long, warm, humid summers (May to October) and mild, dry winters (Hardie, 1977). The annual average temperature is 25 °C and the annual rainfall ranges from 65 to 230 cm, with an average of 130 cm per year (Hardie, 1977; Maloof and Grotzinger, 2012). QuikSCAT satellite observations provide wind speed and direction for the period January 2013 through January 2014 (Harris et al., 2015). The trade winds originate primarily from the east (Fig. 3A) and are strongest and most dynamic during March and April. Throughout a period of 2.5 years, tides in the vicinity of the tidal flats were found to be semidiurnal (Ginsburg and Hardie, 1975; Geyman and Maloof, 2020). Tidal height determines whether the various sub-environments of the tidal flats will be flooded or left exposed. The tidal height measured by Hardie (1977) in a channel mouth and ponds of the tidal flats was 46 cm and 29 cm, respectively. Similar values were measured with tide gauges over a multi-day period in 2017 and 2018 at the Three Creeks site by Geyman and Maloof (2020), see their Fig. 1F. Hardie (1977) illustrated how tidal heights are strongly modified by wind speed, direction, and duration, and Geyman and Maloof (2020) elegantly showed the spatial heterogeneity of tidal flow across the platform top immediately surrounding Northern Andros.

The Bahamas is situated in the main track of West African tropical cyclones (hurricanes). Andros Island is hit by a hurricane on an average of once every 2.5 years, usually between June and October (Hardie, 1977). Notable hurricanes during our study interval include Hurricanes Betsy (1965), David (1979), Arlene (1987), Andrew (1992), Lili (1996), Floyd (1999), Michelle (2001), Wilma (2005), and Matthew (2016). Because they passed in close vicinity to Andros, three of these hurricanes, all major, were included in our analysis (Fig. 3B): a pair of Category 5

hurricanes on the Saffir–Simpson scale – Andrew (1992) and Matthew (2016), and one Category 4 – Michelle (2001). Hurricane Andrew (pink track in Fig. 3B), the strongest tropical cyclone of the 1992 Atlantic hurricane season, developed from a westward tropical wave which moved off the coast of Africa on August 14th and peaked as a Category 5 hurricane while passing over the northern tip of Andros Island with winds of 233 km/h (145 mph) (Major et al., 1996). Michelle (yellow track in Fig. 3B), was the fifth costliest tropical cyclone in Cuban history and the strongest of the 2001 Atlantic hurricane season. It developed from a tropical wave that traversed into the western Caribbean Sea on October 29th, 2001, began to accelerate northeastward, reached its peak intensity as a Category 4 hurricane, then diminished in strength but still maintained winds of 129 km/h (80 mph) over Andros Island (Rankey et al., 2004). Lastly, Hurricane Matthew (green track in Fig. 3B) is the most recent Category 5 Atlantic hurricane to have passed over Andros. Matthew developed into a tropical storm in the eastern Lesser Antilles on September 28th, 2016. After several landfalls in Haiti and Cuba, it weakened somewhat but re-intensified as it tracked northwest, making landfall in the northern Bahamas on October 5th, 2016, with winds of 225 km/h (140 mph) over Andros Island. The storm then travelled parallel to the southeastern coast of Florida over the next 36 h (Stewart, 2017).

3. Material and methods

3.1. Pre-processing of tide-gauge data

The recent sea-level history for the Bahamas was reconstructed for the period 1985–2018 and processed into annual averages (dots in

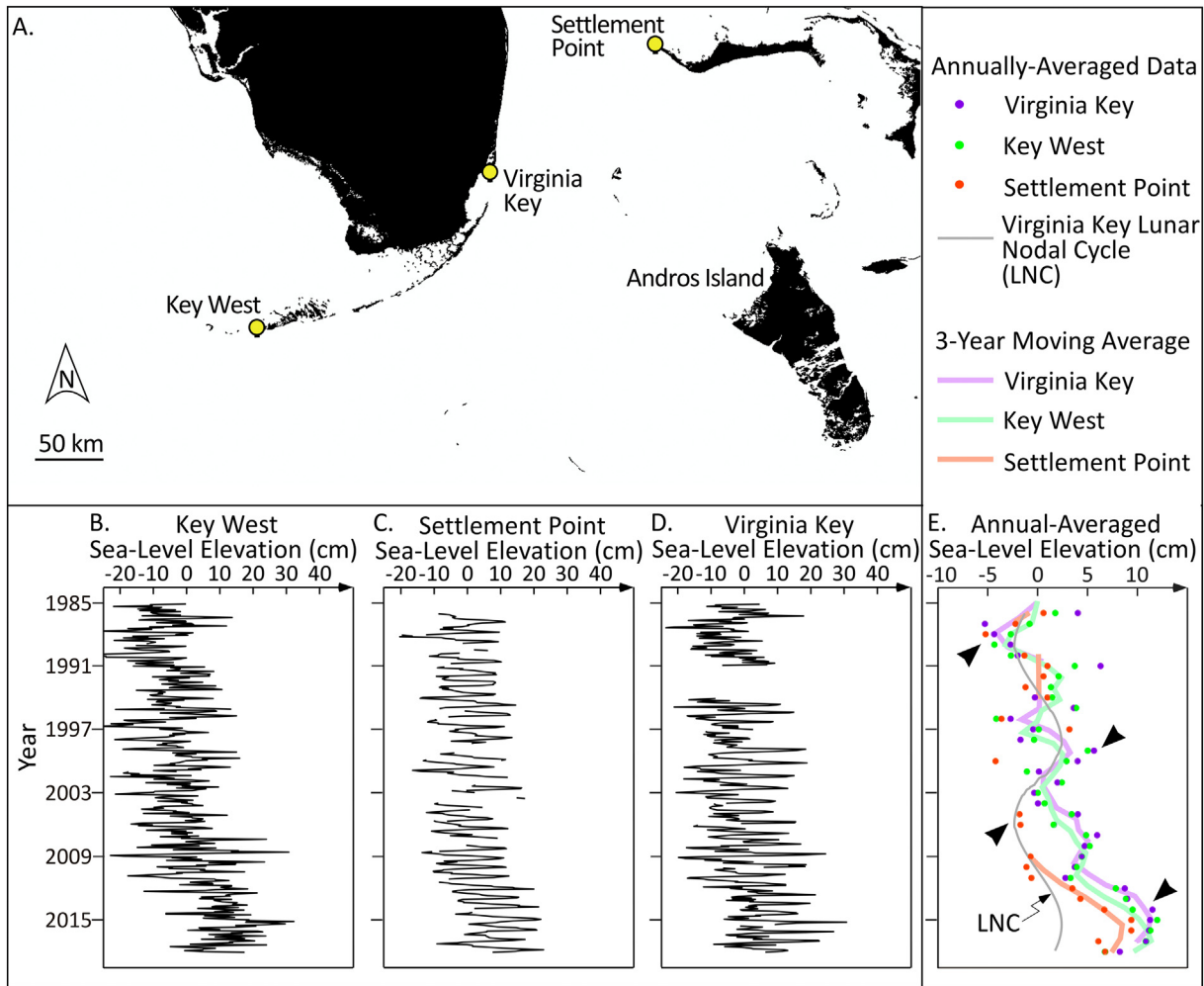


Fig. 4. Sea-level elevations recorded from 1985 to 2018 for three tide gauge stations: Key West, Settlement Point and Virginia Key. (A) shows the locations of the three tide gauge stations, which are the most proximal research-grade tidal gauges to Andros Island. (B–D) show monthly raw sea-level fluctuations in the period 1985–2018. Monthly raw data was then processed into annual averages (dots) and 3-year moving average trend (thick lines) in (E). Note how the 18.61 year lunar nodal cycle (LNC), demarcated by the thin gray line in (E), serves to amplify sea-level rise when in phase with the sea-level fluctuations induced by other factors, but dampens it when out of phase (denoted by black arrows).

Fig. 4E) from an array of the three most proximal research-grade tidal gauges to Andros Island (Fig. 4A–D). The raw monthly tide-gauge data were processed to eliminate daily and seasonal fluctuations due to coastal ocean temperatures, salinities, winds, atmospheric pressures, and ocean currents. A smoothed sea-level trend was also reconstructed from the raw data via application of a 3-year moving average (Fig. 4E). In addition, the lunar nodal cycle (LNC) was extracted from the average of the three sea-level curves. The LNC is produced by the varying declination of the Moon over a period of 18.61 years and drives changes in tidal amplitude globally (Baart et al., 2012). The LNC is important as it amplifies sea-level rise during its ascending phase but dampens rise during its descending phase (Fig. 4E). These effects can exceed 2 cm of relative sea level, which is substantial considering that the linear relative sea-level trend measured in the Settlement Point data was between 0 and 5 mm year⁻¹ at the 95% confidence interval (data provided by tidesandcurrents.noaa.gov). The range of the sea-level rise (~10 cm) documented in this study is reassuringly comparable to that (~8 cm) observed by Rankey and Morgan (2002).

3.2. Pre-processing of vintage aerial photographs

Negatives of vintage 1943 aerial photographs were scanned at 600 pixels/cm to yield digital images with an effective spatial resolution of 1.0 m (Purkis et al., 2016), e.g., Three Creeks in Fig. 5A and B. These photographs were acquired by the British Royal Navy during World War

Two, subsequently used for training by Shell Development Company in the 1950s and 60s and rediscovered in the archives of Robert N. Ginsburg. The shortcoming of these vintage photographs, however, is that they do not contain any geo-information and have to be corrected via georectification, a transformation process used to project an unpositioned (or poorly positioned) historical image onto a known coordinate system. This procedure involves pairing the archive data with a well-positioned satellite image and selecting points on the ground common to both. These locations become reference points in the subsequent warping of the unpositioned image onto a coordinate system. This task was performed in ArcGIS 10.7 through selecting easily recognized ground-control points, which were presumed to have temporal stability, such as blue holes, main channels and ponds, in both the vintage aerial photographs and modern (2018) WorldView-2 satellite imagery. Comparison with GPS readings made in the field revealed the error generated by georectification to be <2.0 m.

3.3. Pre-processing of satellite images

The satellite imagery assembled for the Andros tidal flats were selected every three years for the period 1985 to 2018 within Google Earth Timelapse (Fig. 5C–N). Google Earth Timelapse is comprised of 35 cloud-free annual global mosaics from 1984 to 2018 gathered by the Carnegie Mellon University CREATE Lab's Time Machine library, which has a technology for creating and viewing zoomable and

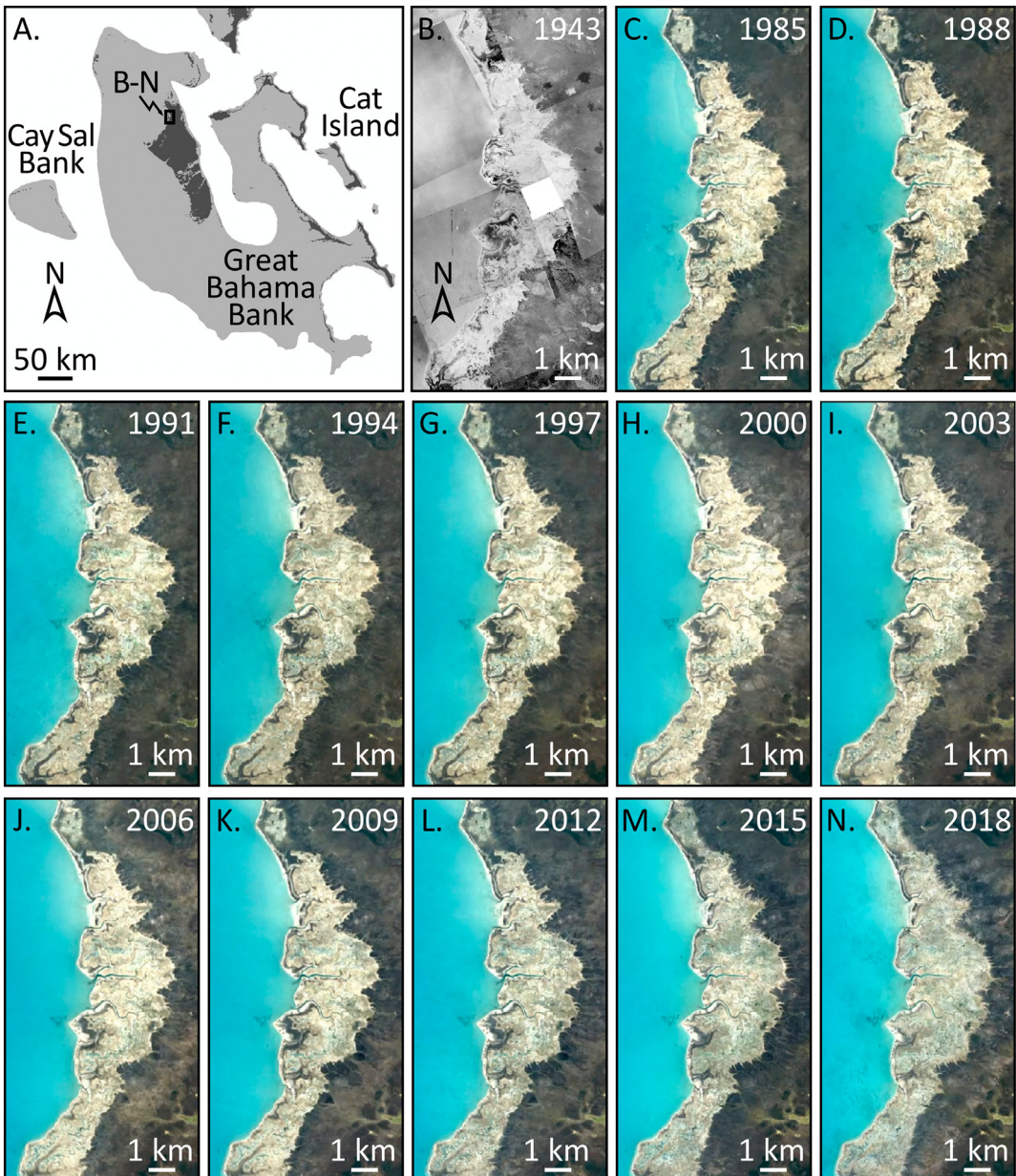


Fig. 5. The study employs time-separated remote sensing images spanning 1943 through 2018 as shown here for the Three Creeks area of the Andros tidal flats, denoted by the black box in (A). The oldest imagery is aerial photographs acquired by the Royal Navy during World War Two, assembled into a mosaic in (B). Data acquired by the NASA Landsat Program are used for imagery spanning 1985 through 2012 (C through L), whereas ESA Sentinel-2A imagery (M) and DigitalGlobe (now Maxar Inc.) Worldview-2 imagery (N) are used for 2015 and 2018, respectively.

pannable time-lapse images. The majority of the satellite data come from Landsat, a sensor which was first lofted in 1972. In 2015–2018, imagery from Landsat 8 and Sentinel-2A (part of the European Space Agency's Copernicus Earth Observation Program) was combined to deliver high-resolution optical imagery which excellently complements data continuity, as provided by SPOT and Landsat images. As the resolution of satellite imagery captured in 1980s–2000s ranges from 5 to 10 m/pixel, the geo-positioning of the imagery was checked against a 2018 WorldView-2 satellite image using ArcGIS (10.7) and deemed to be correct.

3.4. Change detection from time-separated remote sensing of the Andros tidal flats

Shinn et al. (1969) and Hardie (1977) defined the coastline of the Andros tidal flats as the seaward boundary of the channelized zone

which is demarcated by the transition into the subtidal platform interior of GBB. The landward boundary of the channelized zone, meanwhile, is represented by the transition into the inland marsh. As developed in Fig. 1, both boundaries are spectrally distinct and could be reliably digitized in the assembled portfolio of satellite imagery. Because the boundaries of the channelized zone are particularly crisp within the remote-sensing data, this analysis was conducted in four focus areas of 280 km², each distributed along strike down the length of the tidal flats. From north-to-south, these focus areas are Three Creeks, Blue Creek, Middle Bight, and Cormorant Point (Fig. 6B–E). Three Creeks is an example with a well-developed channel system, similar to a configuration that may have been more globally abundant during much of Earth history (Malloof and Grotzinger, 2012). The Three Creeks area is the most often visited locality of the Andros tidal flats and has been examined by sedimentologists since the 1960s (Shinn et al., 1965, 1969). The second of the focus areas, Blue Creek, was selected because it

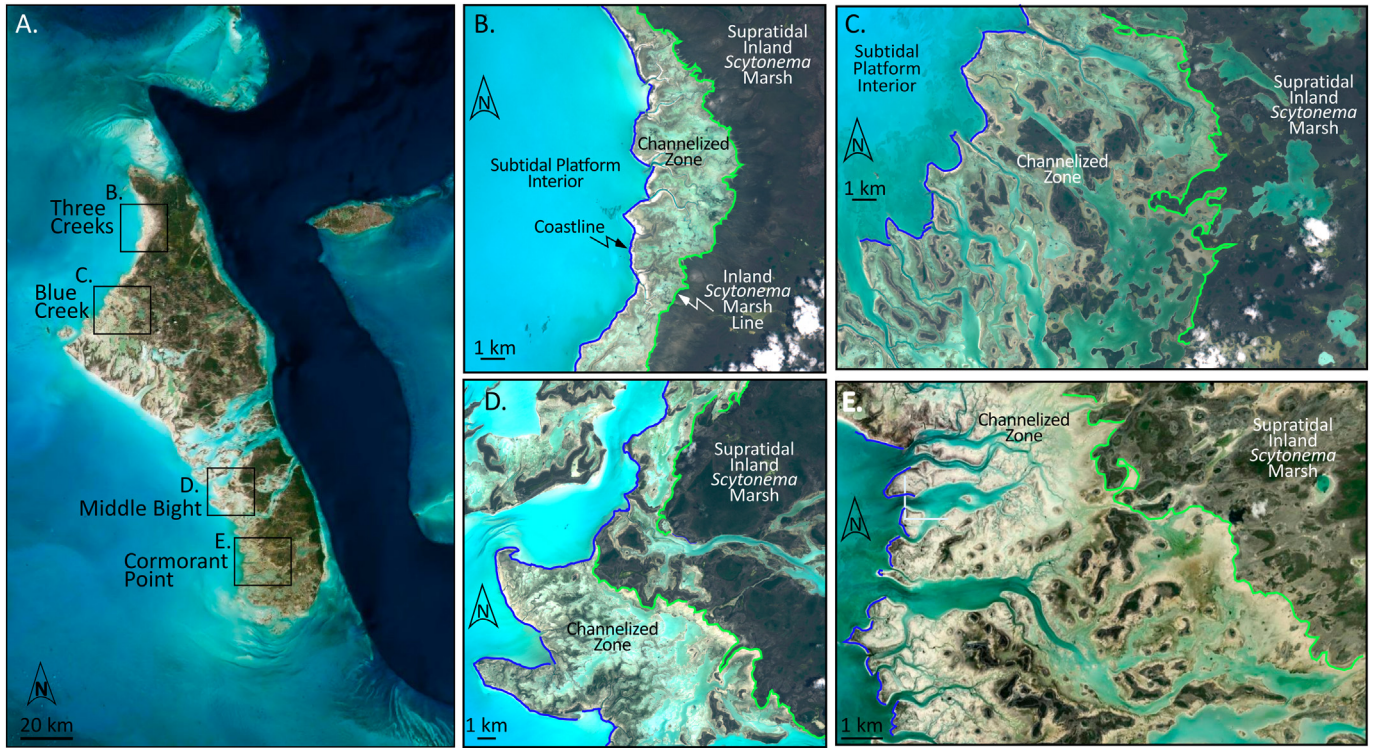


Fig. 6. Analysis of the migration of the boundaries of the channelized zone was conducted in four focus areas, shown in (A) to be distributed from north to south along the western coastline of Andros Island – Three Creeks (B), Blue Creek (C), Middle Bight (D), and Cormorant Point (E). These four areas as illustrated by their respective close-up satellite images capture variation within the channelized zone as well as varying orientation of the coastline with respect to prevailing hydrodynamic energy.

hosts a particularly well-developed and expansive (11 km wide) channelized zone. Further, the *Scytonema* patches in the channelized zone are excellently resolved throughout the Google Earth Timelapse (Fig. 2). The third and fourth focus areas, Middle Bight and Cormorant Point, respectively, are located on the rarely-studied southwest coast of Andros Island and have coastlines which are orientated differently than the other two focus areas, thereby providing contrasting hydrodynamic conditions (Fig. 6D–E).

Changes in the position of the seaward and landward boundaries of the channelized zone were quantified from the period of 1985 through 2018 in the four focus areas using the Digital Shoreline Analysis System (DSAS), an extension to ArcGIS (Thieler et al., 2009; Ford and Kench, 2015). A reference baseline was used as the originating point for the orthogonal transects cast by the DSAS software. The transects intersect the seaward and landward boundaries of the channelized zone establishing measurement points, which were then used to calculate distances and rates of change, every 30 m, for the full length of the tidal flats. Within the channelized zone, changes of the patterning of *Scytonema* patches were manually digitized in the time-separated remote sensing data within the same focus areas. The annualized changes of area and number of the patches were assessed. Dynamics of all these *Scytonema*-dominated facies were considered in the context of recent changes of relative sea level (Fig. 4).

3.5. Quantifying temporal change in the configuration of the tidal channel network

Adapting the workflow of Harris et al. (2011), the network of tidal channels which incise the Andros tidal flats was captured by developing a skeleton of vectors which define the principal axes of the channels. Each element of the skeleton corresponded to the midline of every channel which could be resolved from the high-resolution remote-sensing data. The midline was defined as having equal distance from both sides of the considered channel. Channel skeletons were generated

for the tidal network as resolved in 1943 from the vintage aerial photographs and in 2018 in the modern satellite imagery. The vintage and modern channel skeletons were quantitatively compared to detect changes in the overall length of the channel networks through time, and to identify cases where channels have been created and abandoned during the period of observation.

The data extracted from the vintage aerial photographs (1943) and the modern satellite imagery (2018) were assembled to represent the length of the tidal network in four detailed subareas within the Three Creeks sector of the tidal flat (Fig. 7A). In the same vein as a Strahler number (e.g. Shreve, 1966), each element of the channel skeleton was attributed to one of five orders on the basis of the number of bifurcations separating the considered channel from the ‘main’ channel, defined as connecting the overall network to the coastline of the tidal flats (Fig. 7B–E). This construct delivered a channel-bifurcation hierarchy, whereby the main channel was designated as ‘Order 1’ (red in Fig. 7) and successive bifurcations from which were appended Orders 2 through 5. Order 2 (orange in Fig. 7) are the branches of the Order 1 channels; and Order 3 channels (green in Fig. 7) are branches of the Order 2, and so on.

4. Results

4.1. Migration of the boundaries of the channelized zone through time

Digitization of the coastline and inland marsh line, which demarcate the boundaries of the channelized zone, reveals migrations that can be related to changes in prevailing conditions over the last 33 years (Fig. 8). The inland marsh line in the Three Creeks focus area migrated up to 80 m island-ward between 1985 and 2012. Since the coastline of this focus area only migrated island-ward by ~40 m, the breadth of the channelized zone of Three Creeks increased during this period. The three remaining focus areas – Blue Creek, Middle Bight, and Cormorant Point – behave in accordance with one another and are different to the

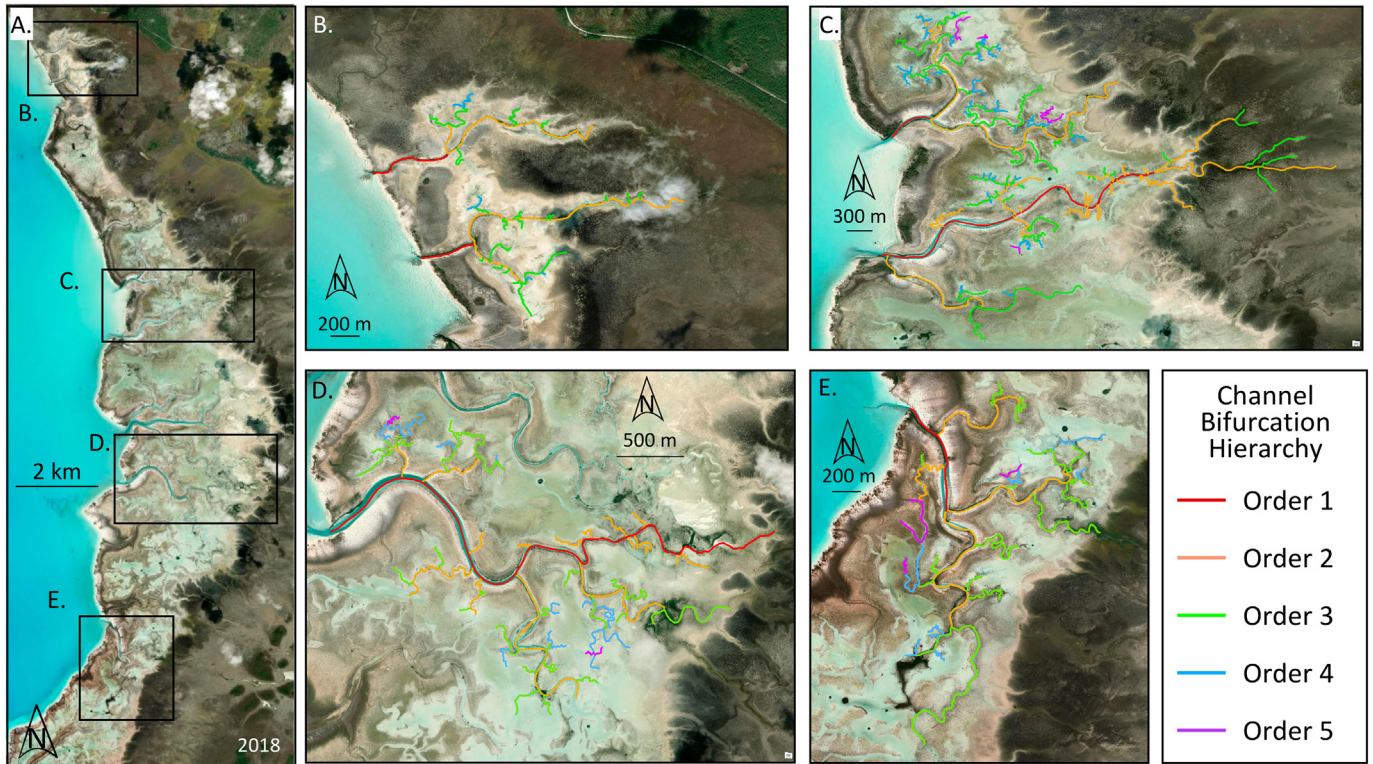


Fig. 7. Boxes in (A) shows the locations of four detailed subareas within the Three Creeks sector of the tidal flats (B–E) where channel bifurcation hierarchy was analyzed. Channels were classified according to their number of bifurcations that link back to the 'main' Order 1 channel which feeds the network from the coastline (text for details) and temporal changes assessed by time-separated remote sensing. (For interpretation of the references to color in this figure, the reader is referred to the web version of this article.)

behavior observed in Three Creeks. For these three, the width of the channelized zones remained unchanged from 1985 through 2012. After 2012, however, the inland marsh lines migrated eastward by 70 m in the Blue Creek focus area, 220 m in Middle Bight, and 190 m in Cormorant Point, observations consistent with threshold behavior. In contrast, the coastlines of these three focus areas remained unchanged throughout the period of observation. Consequently, this migration

produces a meaningful broadening of the channelized zone. Overplotting the arrival of the major hurricanes which impacted Andros Island in the period of observation (Fig. 8) supports the notion proposed by Rankey et al. (2004) that hurricanes do not exert meaningful sway over the evolution of the architecture of the Andros tidal flats. Comparing the movement of the boundaries of the channelized zone with prevailing sea level (Fig. 8A), however, shows a conspicuous relationship.

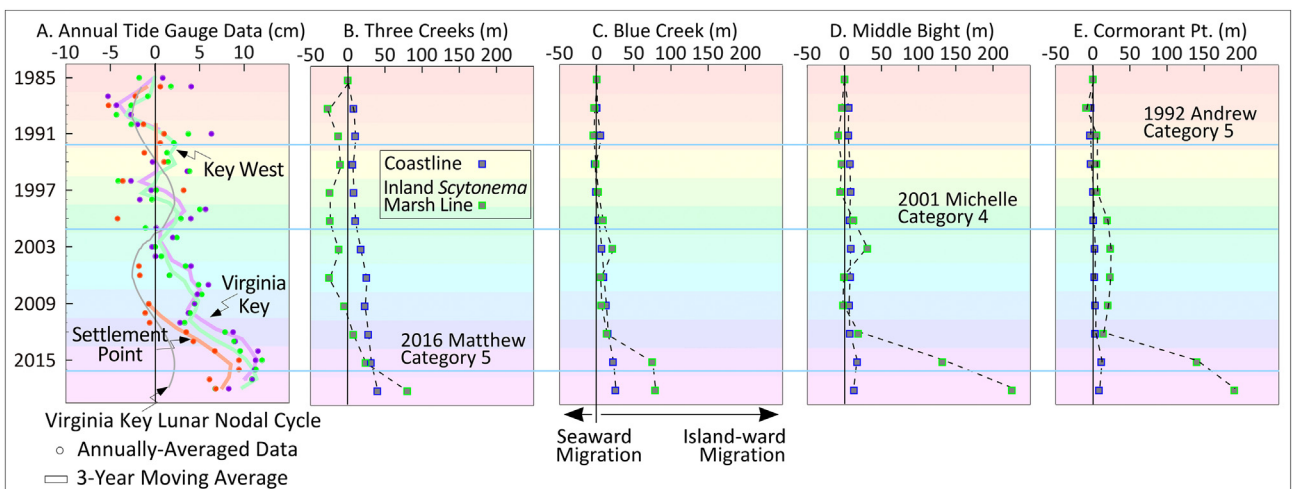


Fig. 8. (A) shows the sea-level history in the region for the period 1985–2018 as quantified by the three most proximal research-grade tidal gauges to Andros Island (Key West, Virginia Key, and Settlement Point, Fig. 4). With all situated within 400 km of Andros Island, data from these sites is considered representative of the long-term sea-level trend. (B–E) chart the migration of the boundaries of the channelized zone – the coastline and the inland marsh line – in the four focus areas normalized to their position in 1985. Note that '0' on the x-axes demarks the position of the coastlines and inland marsh lines in 1985. Positive values on the x-axes of these plots therefore represent the case that the boundaries of the channelized zone (see Figs. 1 and 6) migrate in an island-ward direction (retrogradation), relative to their position in 1985, whereas negative values represent seaward migrations (progradation). Horizontal blue lines in (A) through (E) mark the arrival of major hurricanes that impacted Andros Island during the period of observation. (For interpretation of the references to color in this figure legend, the reader is referred to the web version of this article.)

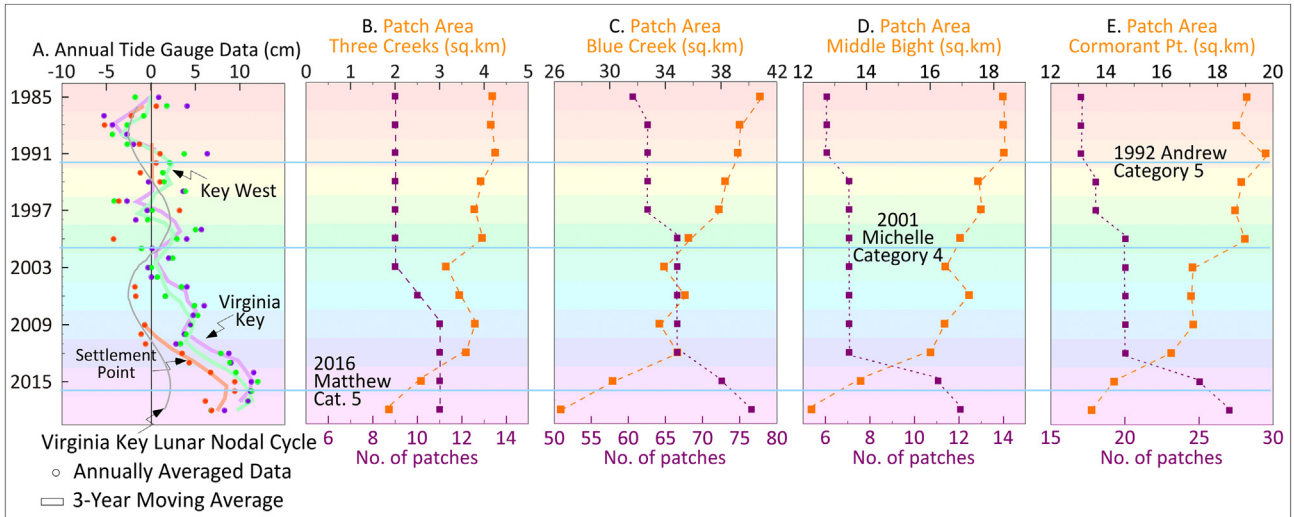


Fig. 9. (A) Sea-level history in the region for the period 1985–2018. The channelized zone of the Andros tidal flats contains *Scytonema* patches, the distribution of which is tracked over the period of observation in terms of their area and number (B) through (E). The timing of hurricanes, over-plotted with horizontal blue lines, appears to have little impact on patch patterning, whereas increases in sea level, first in 2001 and again in 2011, appear to exert meaningful control, leading to fragmentation of the *Scytonema* landscape (text for details). (For interpretation of the references to color in this figure legend, the reader is referred to the web version of this article.)

Although other controls cannot be explicitly excluded, the pronounced expansion of the channelized zone from 2011 onwards corresponds to a subtle but distinct increase in the rate of sea-level rise and increase in overall sea-level amplitude, which peaked in 2015. Note that the expansion of the channelized zone slowed at this time in the Blue Creek focus area but continued unabated at Middle Bight and Cormorant Point.

Temporal changes in the patterning of *Scytonema* patches were assessed on the basis of tri-annual tallies of their quantity and size within the four focus areas (Fig. 9). As with the migration of the boundaries of the channelized zone, the patch dynamics within the four areas cannot be related to hurricane impacts, but they do develop in step with the cumulative sea-level changes, suggesting a causal relationship. If rising sea level is indeed exerting sway over the patterning of the *Scytonema* patches, its control is more nuanced than for the migration of the boundaries of the channelized zone. For instance, the major 2012–2015 episode of sea-level rise was proceeded by a lesser rise which peaked in 1999, approximately coinciding with the arrival of Hurricane Michelle (Fig. 9A). Although this first peak does not impact the breadth of the channelized zone (i.e., Fig. 8), it does front a marked decrease in the size of the zone's *Scytonema* patches, signaling the early stages of the shrinkage of this landscape. The second sea-level peak (2012 onwards) corresponds to a renewal, indeed acceleration, of the decrease in area of the patches across all four focus areas, but also precipitates a radical increase in the number of patches (Fig. 9B through E). This trend can be interpreted to represent the wholesale fragmentation of the localized supratidal highs in the channelized zone (for which the presence of *Scytonema* is a proxy). This change might be considered to have been induced by the fact that sea level has risen beyond a critical threshold for the stability of this cyanobacterial-dominated landscape to be maintained (a tipping point – e.g. van de Vijsel et al., 2020).

4.2. Temporal change in the architecture of the tidal channels

Analysis of the evolution of the tidal creeks in the vicinity of Three Creeks reveals substantial changes occurred between 1943 and 2018. As captured by Fig. 10C, in all subareas save for that situated in the southern reaches of Three Creeks, the length of the channels created between 1943 and 2018 greatly exceeds those lost in the same period due to channel abandonment. Hence, the channel network in these three areas is becoming more extensive with time. Partitioning the data into

five orders of bifurcation reveals that the increase in the length of channels is concentrated in bifurcation Orders 3 and 4. No changes are observed for Order 1. The southernmost focus area is distinct in that there is a 1.6 km reduction in the length of its third-order channels, which exceeds the sum of the lengths of the increased extension of the third through fifth order channels. However, if the exceptional third-order behavior is excluded, the length of fourth- and fifth-order channels created is longer than those abandoned. If the behavior of the tidal channels is plotted against the breadth of the channelized zone (Fig. 10D) and direction that the coastline of the four detailed study areas face (Fig. 10E), it can be seen that the two areas whose channels are the most dynamic through time (i.e. the pair situated in the middle of Three Creeks) are also the areas where the channelized zone is at its broadest, whereas the southernmost area with its distinct behavior is the only one oriented perpendicular to the passage of winter cold fronts. These observations suggest that increased channel dynamics might be anticipated in areas where the channelized zone is best developed, and if the zone broadens through time (as suggested by Fig. 8), that channel dynamics will increase in step with rising sea level.

5. Discussion

5.1. *Scytonema*-dominated facies respond swiftly to rising sea level

Scytonema is a dark-filamented, large (individual filaments 10 to 30 µm in diameter) cyanobacterium, primarily a freshwater lover, that grows in stubby upright tufts several millimeters to a few centimeters in height (Black, 1932; Monty, 1972; Hardie, 1977; Fig. 11A and B). The near-surface sediment below the *Scytonema* mat is densely layered from millimeter-laminae to cm thick beds (Fig. 11B) (Hardie, 1977). Tracking the change in the configuration of *Scytonema* mats through time serves as a sensitive proxy for changes in sea level because this genus of cyanobacteria is biologically bound by a specific point in the tidal range, e.g., approximately 7 cm below mean high water per Hardie (1977). Such high-elevation areas allow these tidal-flat portions to be relatively free from the day-to-day tidal fluctuations (Hardie, 1977; Hardie and Ginsburg, 1977). The cyanobacteria create expansive black mats that extend within the inland marsh 4–8 km eastward abutting the Andros pineland perched atop the exposed Pleistocene limestones of the island (Fig. 1B and C) (Shinn et al., 1965; Hardie, 1977). Although *Scytonema* patches also develop in the levee-pond complex

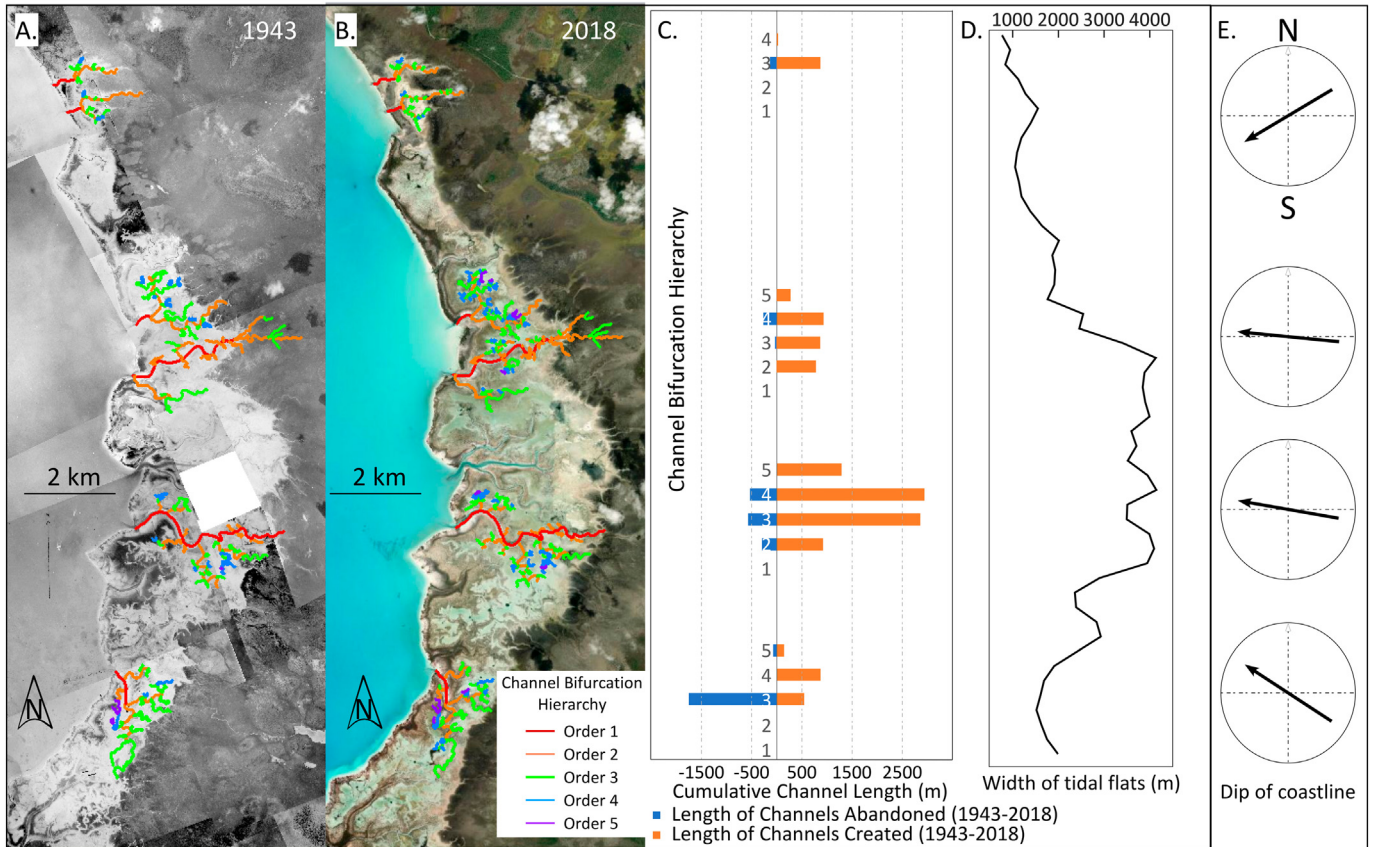


Fig. 10. Changes to the morphology of the channel network assessed in the four detailed subareas within the Three Creeks sector of the Andros tidal flats in the period 1943 through 2018. (A) and (B) map the channel bifurcations, color-coded by their hierarchy (text for details) for the four areas in 1943 and 2018, respectively. (C) charts the cumulative length of the channels gained and lost in this time period, by bifurcation hierarchy. Note that the greatest changes are observed in the two central areas where the tidal flat is broadest (D) and where the coastline is west facing (E). (For interpretation of the references to color in this figure legend, the reader is referred to the web version of this article.)

in the channelized zone, they dominate the island-ward portion of the channelized zone and are fully developed within the supratidal zone. With the help of Google Earth Timelapse, the annual differences in the changes of *Scytonema* growth patterns can be detected using GIS tools.

After deducting the differences caused by the winter and summer seasons, the rate of change was calculated between the two facies: *Scytonema*-dominated patches in the channelized zone, and the non-*Scytonema*-dominated facies of the coastline and remaining parts of the channelized zone. Their contrasting rates of change through time could then be related to external forcings. Although other controls cannot be discounted, the temporal change in patterning of the *Scytonema*

patches seems to respond in a way which is compatible with meaningful control being exerted by the ~10 cm rise in sea level that occurred during the period of observation. A plausible mechanism for sea level driving this change can be formulated. With sea-level rise, incoming seawater flows through the tidal channels and into the ponds, thereby increasing the salinity of any ponded water (Hardie, 1977). When pond salinity exceeds one part per thousand, the colonies of sensitive *Scytonema* begin to decay in size and fragment (Black, 1932). Hardie (1977) showed that *Scytonema* can tolerate no more than 4–5 days of continuous submergence in seawater. Any colonization, even a centimeter or two below the critical surface elevation, where the



Fig. 11. (A) A surface view of tufted *Scytonema* mats. (B) shows the sediment immediately below the surface, which is densely layered from millimeter-laminae to cm-thick beds. (C) shows the light colored, cohesive *Schizothrix* mats and fresh layer of lime mud locally covering levees developed along tidal channels. (For interpretation of the references to color in this figure legend, the reader is referred to the web version of this article.)

submergence time abruptly doubles between the mean high-water neaps and mean tide level, will be exposed to at least one lethal dose (more than nine days) of seawater each year (see Fig. 93 in Hardie, 1977). A ~10 cm rise in sea level is seemingly sufficient to affect the channelized zone and lead to the wholesale change of the *Scytonema*-dominated areas. Whereas sea-level rise is a plausible driver of change in this facies belt, we acknowledge that rise can be induced globally as a eustatic signal, but also initiated locally via differences in wind-setup, for instance. Changes in patterning of the *Scytonema* patches should be anticipated to be agnostic to the cause of sea-level rise and for this reason, we caution against interpreting patch fragmentation alone as a signal of regional sea-level change. Fig. 8B depicts the largest islandward coastline migration of 40 m at the Three Creeks site, as compared to other three focus areas. Though the island-ward migration (erosion) of the coastline is anticipated as a consequence of sea-level rise (Pethick, 2001), any migration is mostly due to the mixed and complex physical-induced processes that depend on the offshore hydrodynamic sub-environments, including wind direction and sediment supply (Hernández-Cruz et al., 2006; Taylor and Purkis, 2012; Purkis et al., 2016; Kench and Mann, 2017; Duvat, 2019). In winter, the Andros tidal flats experience intermittent winds from the north as cold fronts move southward. The E-NE facing Three Creeks area takes the brunt of these winds while the southern Andros tidal flats are in the lee. Thus, a higher amount of erosion and coastline migration - within the framework of rising sea level - is expected along this portion of the Andros tidal flats.

Black (1933), Gebelein (1969), and Hardie (1977) emphasized a vital role played by an additional smooth, tough and rubbery mat formed by the cyanobacterium *Schizothrix*, which, in contrast to *Scytonema*, can tolerate seawater salinities for extended periods of time. This pink–gray cyanobacteria with filaments <5 µm in diameter locally cover beach terraces and channel levees of the channelized zone (Fig. 11C). This type of mat is a pervasive sediment-binding filament complex, because its trichomes can exit their sheaths and migrate above newly-deposited mud to avoid burial and seek sunlight. Repetitive flooding of beach ridges and levees with sediment-laden storm waters and the subsequent binding by *Schizothrix* form laminations ranging from 0.1 to 2.0 mm in these sub-environments (see Hardie, 1977; his Figs. 34 and 43). According to the observation of Black (1933), Gebelein (1969), Hardie (1977), and Hardie and Ginsburg (1977), *Schizothrix* forms soft, gelatinous mats within in which particles ranging from mud to sand size are trapped and bound extremely tightly, to the point that it protects the underlying sediment from significant erosion during spring high tides, hurricane floodings, or rain wash. Therefore, the cohesive nature of sediments along the coastline partly explains its static character (as captured in Fig. 8). *Schizothrix* also occurs along channel levees and likely retards erosion and migration of channels. *Schizothrix* patches are, unfortunately, difficult to resolve via remote sensing data because the patches along the beach terrace and levee crests are narrow (10–30 m) and their pale color is spectrally indistinguishable from the background pelleted mud.

5.2. Tidal flat facies record sea-level change in the rock record

This study has quantified the dynamic changes of boundaries of tidal flats (the coastline and an internal boundary) at timescales relevant to the projections of the tidal-flat architecture in the rock record. Whereas the Andros tidal flats have experienced a ~10 cm sea-level rise over the 75 year period of observation, we are cognizant that this rise is one to two orders of magnitude swifter than that which might have been encountered in the deep-time ancient record, with the offset being particularly acute when considering greenhouse worlds. While keeping this caveat in mind, we believe that our results still capture important learnings. The results of this study show that the changes in the positions of the landward boundary of the channelized zone respond more dramatically to rising sea level than the seaward boundary does. As the

channelized zone widens by extending further into the supratidal area, subtle changes leave evidence that would potentially allow sedimentologists to recognize products of a change in the rate of rise of sea level in the rock record. Our remote sensing study cannot eliminate the possibility of other controls on tidal-flat architecture operating during the 75 year excerpt in the history of the evolution of the Andros tidal flats that we have examined. Whereas pronounced episodes of sea-level rise appear to lead the broadening of the intertidal channelized zone, the lengthening and avulsion of the network of tidal channels that traverse this zone, and the fragmentation of the *Scytonema* patches which inhabit it, experience would suggest that the facies belt is responding in a complex and non-linear fashion to a myriad of controls. Among these, sea-level rise seems to be a relevant control and possibly a dominant one. In particular, since our data excludes storm activity as a major contributor.

The Holocene sediment record of the tidal flats is predominantly of bioturbated, unlaminated, pelleted carbonate mud and silt. Layered sediment exists only as a thin cap over bioturbated sediment in the channel belt and as thin-bedded inland marsh sediment. Homogenization of layered sediment by marine organisms is a major sedimentary process on subtidal and intertidal parts of the tidal flats. Layering is preserved where burrowing organisms are excluded by prolonged exposure above sea level (Hardie and Ginsburg, 1977); the crest and backslope of the levees are exposed over 90% of the time, the ponded areas only 10% to 60% of the time. The duration of subaerial exposure largely controls: (1) variations in the cyanobacterial mats and resultant physical layering of sediments; (2) formation of intraclasts and mud clasts by desiccation; and (3) burrowing by crustaceans, worms, and insects.

Combined with the dynamics of the boundaries of the channelized zone (Figs. 8, 9, and 10) and fluctuations of sea level (Fig. 4), the sedimentologic record of sea-level rise can be evaluated at three positions in the channelized portion of the tidal flat. The most seaward location of the coastline (Fig. 1) remained relatively static after the establishment of the tidal flats, even when sea level continued to rise. Therefore, a rising sea level might increase the thickness of the tidal-flat deposits, but not change their sedimentology (in terms of rock type or sediment structure) at this first location. At the coast, however, local erosion of the beach ridge and of the underlying mudstone has occurred, and in these sites, the presence of intraclasts and minor transgression of subtidal facies would therefore be anticipated. More noticeable signs of a change are found in areas at the center and landward portions of the channelized zone. Two types of evidence for a sea-level rise should be anticipated in the center of the channelized zone: in some areas, channel deposits (e.g., intraclast- and skeletal-rich channel lags) might be produced in the new layer of sediments corresponding to a lengthening of the channels. In inter-channel areas, meanwhile, a decrease in the prevalence of the thickly laminated to thin-bedded facies should be envisaged, due to the fragmentation and reduction of the *Scytonema* patches, which would be succeeded up-section by an increase of bioturbated pelleted mud. Considering the hundreds of meters of migration of the landward boundary of the channelized zone (as demonstrated in Fig. 8), the landward portion of the channelized belt would likely represent the site of greatest change, wherein the thinly bedded and laminated inland *Scytonema* marsh would be overlain by sediments of the channelized zone, which is characterized by bioturbated mud, patches of *Scytonema*, and localized channel deposits.

Aspects of these hypothetical sedimentary records are reinforced by a core sample collected in one of the abandoned channels in the Three Creeks area in April 2019 (Fig. 12). Concentrated gastropod shells accompanied by wackestone and packstone textures in Fig. 12G are considered as the signature of the now-abandoned channel. Core descriptions of the layering in the Andros tidal flat (e.g., Black, 1933; Shinn et al., 1969; Hardie and Ginsburg, 1977), as well as other modern carbonaceous tidal flats (e.g., Illing and Wells, 1964; Kendall and d'E. Skipwith B, 1968; Davies, 1970; Logan et al., 1974), further support

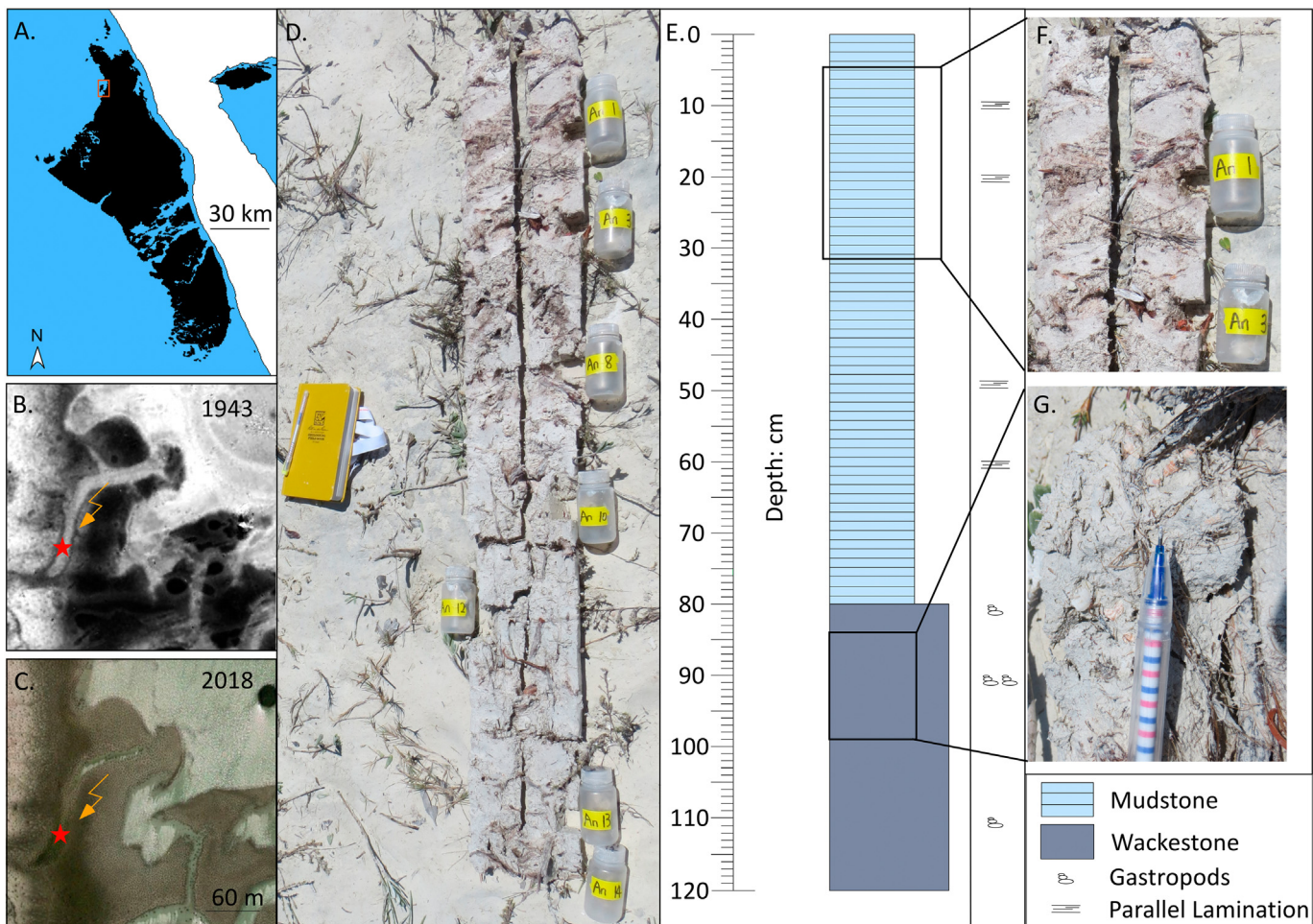


Fig. 12. A core sample collected in one of the abandoned channels in the Three Creeks area (A). The channel was active in 1943 (B) but abandoned in 2018 (C). (D–E) show the 120 cm-long sediment core with photograph and description, respectively. In the core, laminated mudstone (F) extends from 0 to 80 cm and overlies gastropod-rich intermixed wackstone to packstone (G). The concentrated gastropod shells (in G) and grainier textures are considered as remnants of the channel.

the hypothetical records. The laminations in the geologic record represent a response to recurrent or rhythmic change in the sub-environment of alternate flooding and draining (Black, 1933). Illing and Wells (1964) and Purkis et al. (2017a, 2017b) noted the exclusive development of lamination at the intertidal cyanobacterial mats in the Qatar area of the Persian/Arabian Gulf. They reported that these 'stromatolitic algal laminations' could be used to recognize the buried tidal flat environment beneath the supratidal sabkha. Shinn et al. (1969) observed that cores taken in the adjacent offshore marine, bars, channels, and ponds of the Andros tidal flats lacked layering, whereas laminations in the levee deposits are well developed and distributed patchily (see their Figs. 3, 6, 9, and 19). Details of the layering styles recognized in the Andros flats were more fully documented by Hardie and Ginsburg (1977).

These many studies of tidal-flat settings convincingly reinforce the notion that well-laminated cyanobacterial mats represent distinctive primary depositional environments and can therefore provide important criteria leading to an interpretation from cores or outcrops. For example, *Schizothrix* laminations near channels are an indication of a local shallowing between subenvironments, reinforcing that small changes in water depth can induce substantial changes in sub-environment. This example and other recent studies (Rankey, 2002; Maloof and Grotzinger, 2012; Geyman et al., 2021) demonstrate that the facies mosaics on tidal flats and their stacking into peritidal parasequences are not random, as proposed by Wilkinson et al. (1997). Different conclusions on randomness need not be contradictory. Random stacking

should not be considered as evidence for a lack of control on the development of the tidal-flat stratigraphy. Rather, randomness suggests a cacophony of numerous controls interacting in a complex way. Whereas we posit that sea-level rise is a dominant force in the evolution of the Andros tidal flats, at the broad scale, during the 75 years that were examined herein it would be foolhardy to assume that sea level is solely dictating facies development. Other controls, such as variation in the spatial and temporal productivity of the lime-mud factory which nourishes the tidal flats (e.g. Robbins et al., 1997; Purkis et al., 2017a, 2017b) are also surely important, as are the interaction of wind, waves, rainfall, and so on, with local topography. Such controls invariably operate at different spatial scales, thereby nuancing their importance at different localities in the overall facies mosaic. Framed as such, it is unsurprising that multiple authors report different degrees of randomness as they consider different portions of the tidal-flat stratigraphy. Recognition of the multiplicity of controls on layering in tidal-flat deposits should always be considered when inferring change in water depth, so as to enable a more accurate interpretation of tidal-flat evolution in ancient carbonates.

5.3. The impact of sea-level rise exceeds that of storms

Previous studies (e.g., Ball et al., 1967; Hardie, 1977; Rankey and Morgan, 2002; Rankey et al., 2004; Maloof and Grotzinger, 2012) have shown sea level and storms to be important agents in the geomorphic evolution of modern carbonate tidal flats. However, the complexity

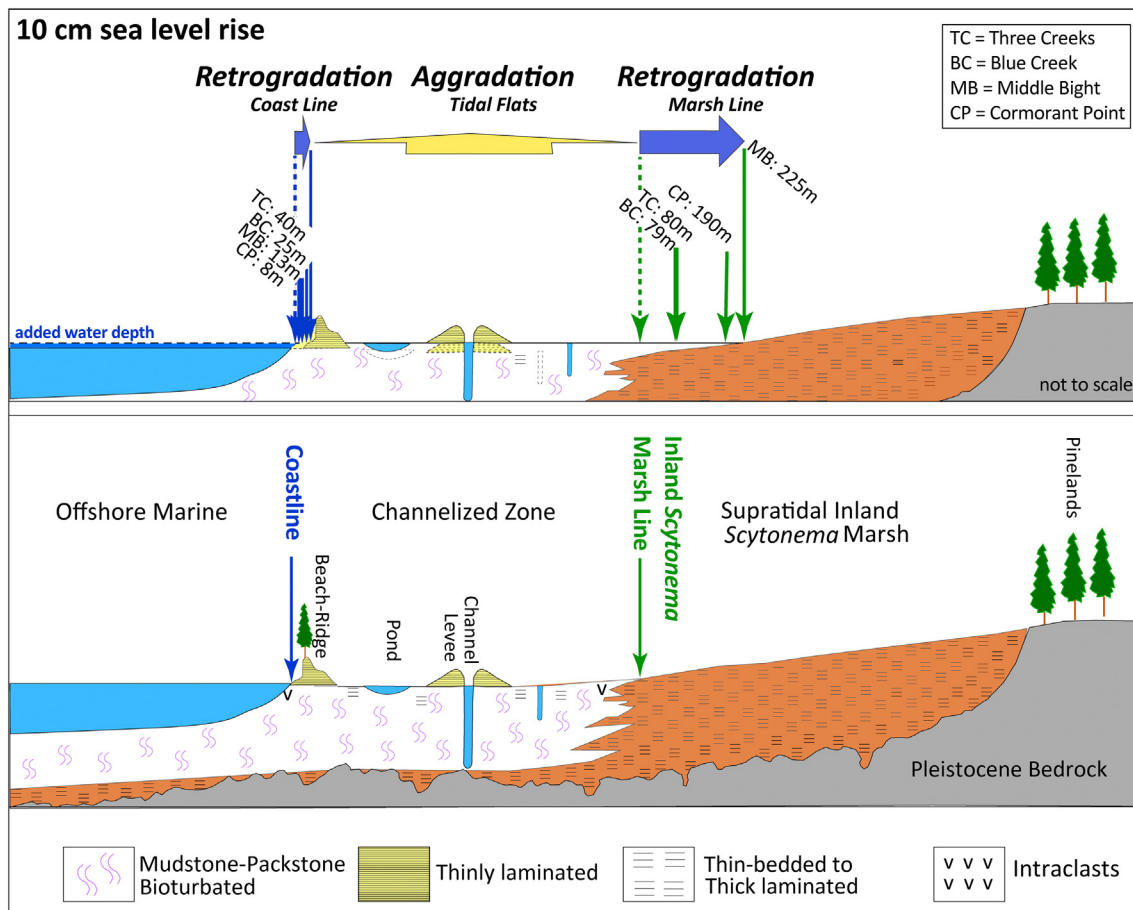


Fig. 13. Short-term evolution of Andros tidal flat complex as documented in this study. Bottom: Schematic cross section based on published field studies and coring highlighting the position of the coastline (blue) and the boundary (inland marsh line in green) between the channelized zone and the supratidal inland marsh. Top: Migration of the coast and inland marsh boundaries after 10 cm of sea level rise that occurred in the last 75 years documenting the variable retrogradation of the facies boundaries. The coastline retrograded between 8 and 40 m while the boundary between channelized and supratidal zones retrograded up to 220 m, pushing the marsh line landward. Aggradation occurs in the channelized zone that leads to higher levees, and as observed in the comparative imagery filling of some ponds and secondary channels. Dashed arrows indicate original position of boundaries. The locations of the four focus areas are displayed in Fig. 6. TC = Three Creeks, BC = Blue Creek, MB = Middle Bight, and CP = Cormorant Point. (For interpretation of the references to color in this figure legend, the reader is referred to the web version of this article.)

and sensitivity of tidal flats complicate the evaluation of the relative impacts of these two physical drivers. This study suggests that sea-level rise exhibits a more pronounced impact than storm events on the evolution of tidal flat facies belts over the short time period analyzed in this study. Plotting of the arrival of hurricanes (Andrew 1992, Michelle 2001, and Matthew 2016, Figs. 8, 9) denies the existence of a relationship between such large storms and the parameters that were analyzed, as indeed has been intimated by previous studies (Perkins and Enos, 1968; Wanless et al., 1988; Boss and Neumann, 1993, 1995; Rankey et al., 2004).

Our results corroborate the findings of Rankey et al. (2004) who, by integrating remote-sensing data with field observations, demonstrated that Hurricane Michelle (2001) had little impact on the patterning of the Andros Island tidal-flat facies mosaic. There are several aspects of any given storm (see Fig. 3) that plausibly can converge to dampen its sedimentologic impact on tidal-flat environments (Wanless et al., 1988; Boss and Neumann, 1995; Tedesco et al., 1995; Risi et al., 1995; Rankey et al., 2004). The height of the wind-driven tide is roughly proportional to the forward speed of the storm; therefore, the duration and impact of storm-related processes would be reduced as a rapidly-moving storm passed over an area, shortening its period of impact (Rankey et al., 2004). Another aspect of storms that relates to impact is the wind speed and wind direction. Hurricane Andrew, for instance, delivered wind speeds of 233 km/h, Hurricane Michelle delivered 129

km/h, and Hurricane Matthew wrought 225 km/h near (or across) Andros Island (Boss and Neumann, 1995; Beven, 2002; Landsea et al., 2004; Stewart, 2017). The wind speed is crucial for the subaerially-exposed areas, but its effect is greatly reduced underwater. For example, during Hurricane Andrew, the northern portion of the Andros tidal flats was inundated by up to 5 m of storm-surge waters. Consequently, the beach ridges experienced minimal erosion, but since the storm surge was laden with mud that was stirred up in the offshore marine environment, Andrew produced an irregular layer of mud up to 1 cm thick across much of northern GBB including the Andros tidal flats (Major et al., 1996). Extrapolating this storm deposit into the deep-time geological record might deliver a sufficiently large thickness of strata for storms to be recognized, even with only intermittent preservation. Boss and Neumann (1993, 1995), by contrast, observed minimal impact of Hurricane Andrew on the sedimentary environments of northern GBB. Storm flooding with sediment-laden waters is maximized with onshore winds. Rankey et al. (2004) postulated that a portion of the southwestern coast of Andros (including Middle Bight) lay within the path of the eye of Hurricane Michelle, thus should have experienced maximum wind velocity (and surge) in an onshore direction, which would have combined to raise the intensity of storm flooding. However, minimal sedimentary impact occurred and the facies boundaries in Middle Bight remained relatively intact. Hurricane Betsy, which impacted the Andros area in 1965, also deposited little sediment on the tidal flats

(Perkins and Enos, 1968), although, in this case, the storm energy moved offshore. Although mud accumulation occurs during hurricanes and therefore their effect should not be discounted, the erosive forces of hurricanes do not shift facies boundaries, at least during the time period documented in this study (Figs. 8 and 9).

5.4. The evolution and future morphology of the Andros tidal flats

There are several reasons why the future morphology and geologic record of the Andros tidal flats should be of interest. One significant reason is that cyclic peritidal carbonates have been inferred many times in the ancient, yet many examples lack sufficient evidence of cyclicity to support the interpretation (e.g. Burgess, 2016). Hence, an understanding of the evolution of the modern tidal flat could improve depositional models. And enhanced models would benefit exploration and development drilling for such subsurface deposits in areas where they contain major hydrocarbon reservoirs, e.g., the Permian Basin of West Texas and New Mexico, and the Mississippian from Saskatchewan (Ginsburg, 1971; Shinn, 1983; Roehl and Choquette, 1985).

Ginsburg's (1971) autocyclic model envisaged that the tidal-flat complex would prograde seaward across a relatively flat and seaward-dipping platform top, assuming a steady subsidence rate and depth-dependent sediment production. Ginsburg (1971) saw his model based on the recent tidal flat-capped cycles in the Bahamas as an alternative to a tectonic explanation of repeated regressive cycles, as, for instance, discussed by Fischer (1964). Stratigraphic-forward models demonstrated that Ginsburg's autocyclic model is a plausible mechanism to generate widespread shallowing-upward cycles or parasequences (Demicco and Spencer, 1989; Goldhammer et al., 1993; Burgess et al., 2001; Burgess, 2001; Zhang et al., 2019). But the results presented herein, as well as those of Berkeley and Rankey (2012) for the modern tidal flats of Crooked Island, south-east Bahamas, underscore the relative stability of tidal flats during a rapid sea-level rise of 10 cm – essentially no progradation occurred. Furthermore, the data presented here document that during the last 75 years, the tidal flats mostly aggraded and the channelized zone retrograded up to 220 m across the supratidal areas (Fig. 13). This rapid expansion of the channelized zone provides strong evidence that the supratidal zone is in fact not prograding.

Such a peritidal facies progradation with a stable coastline is postulated in the recent model for the evolution of the Andros tidal flats by Maloof and Grotzinger (2012). In their model, the tidal flats develop behind a beach ridge that forms early during the Holocene flooding of GBB and, despite some erosion wrought by the continuously rising sea level, the ridge provides a barrier for wave wash and enables mud to accumulate behind it. Tidal channels that cut through the beach ridge bring mud from the offshore into the protected areas, resulting in net landward accumulation of sediment and leading to an eastward expansion of the tidal flats. This portion of the model is corroborated with our analysis of the channel network that is becoming more extensive with rising sea level (Fig. 10). However, Maloof and Grotzinger (2012) also postulate an out-of-phase westward progradation of the supratidal zone, that progressively covers the channelized zone. The data presented herein does not support progradation of the supratidal zone but, to the contrary, indicate a potential shrinking of the supratidal zone as the channelized zone expands landward (Figs. 8 and 13). The results in this study show that the Andros tidal flats did not prograde during the observed Holocene sea-level rise, nor did the supratidal areas prograde over the channelized zone, as proposed in both Ginsburg (1971) and Maloof and Grotzinger (2012). During the current sea-level rise the tidal flats instead generally aggraded and retrograded, with the channelized belt backstepping towards Andros Island. Coastline stability suggests that the seaward boundary of the channelized zone received sufficient sediment during the period of observation to aggrade and maintain position. If ample sediment was supplied during a less-rapid period of sea-level rise, the coastline might prograde. Core borings west of Andros Island, however, have not recovered tidal flat facies in

strata spanning the last 20 million years (Beach, 1995; Manfrino and Ginsburg, 2001; Kenter et al., 2001).

An additional important reason for interest in tidal flats is that low-lying areas like Andros are particularly vulnerable to sea-level rise induced by global climate change. The extreme consequence could be imagined that tidal-flat retrogradation would track with the sea-level rise until the entirety of Andros Island is inundated. However, this scenario is not so straightforward since the elevated Pleistocene limestone ridges under the pinelands portions of Andros Island (Fig. 1) will likely limit the magnitude of easterly retrogradation of the tidal flats. Also, with a rising sea level, the hydrodynamic environment across the GBB, which controls sediment supply and transport to nourish the tidal flats with fine-grained sediment produced in the platform interior to the west, will be modified and changed to no doubt alter the sediment budget, and possibly also the position of the coastline. At the point that continued flooding removes the influence of Pleistocene topography as a “barrier” for creating a lower energy setting in its lee, then the more regional setting that has allowed the muddy tidal flats to form will have been removed and a situation of more open circulation will be initiated. Due to the highly dynamic nature of the tidal-flat environment, and complex hydrodynamic surroundings, sediment and facies monitoring surveys are required if the future evolution of tidal flats is to be understood.

6. Conclusions

This study has implications for the interpretation of tidal-flat environments in the rock record in that it captures the reconfiguration of inter-to-supratidal facies as forced by changes in the rate of sea-level rise. A 10 cm sea-level rise documented during the 1985–2018 period of study for which research-grade sea-level records are available was sufficient to broaden the channelized zone of the Andros tidal flats by up to 220 m and to initiate the wholesale fragmentation of the localized supratidal highs in this zone. It is important to note that the expansion of the channelized zone is driven by the retrogradation of its island-ward margin (the inland marsh line), not by progradation of the coastline, which remains conspicuously stable in the face of rising sea level. We reemphasize, however, that the rate of sea-level rise during the period of observation is conspicuously rapid, even in the context of icehouse conditions. The study also reveals that although the channel network of these carbonate mud-flats lacks the autogenic dynamics of equivalent siliciclastic deposits (e.g., Fagherazzi, 2008; Budd et al., 2016), channels in the inner extremes of the network (i.e., third through fifth order in the bifurcation hierarchy) are dynamic. The cumulative length of abandonments through time is to be surpassed by the creation of new channels. Perhaps counterintuitively, these findings suggest that, while the coastline is relatively insensitive to the increase in sea-level rise, the rise is manifested by wholesale reconfiguration of the channelized zone farther inboard, as the abundance of laminated cyanobacterial (*Scytonema*) fabrics decreases and the cumulative length of tidal channels increases. Through the concept of comparative sedimentology, it is anticipated that these modern observations might be applied to better recognize variations in the depositional record during a sea-level rise in ancient carbonate deposits, even for low-amplitude, sub-orbital sea-level cycles.

Declaration of competing interest

The authors have no conflict of interest to declare and pledge that the submitted work is original.

Acknowledgments

We are sincerely grateful to Robert N. Ginsburg for retaining the vintage aerial photographs on which this study was based. We further extend our thanks to the CSL Center for Carbonate Research within the Department of Marine Geosciences, University of Miami, who have supported us, and to Brian McNoldy (RSMAS) for his help interpreting

tidal-gauge data and the lunar nodal cycle. We are grateful indeed to Juan Carlos Laya Pereira, Jim Markello, Imelda Johnson, and Miles Frazer for unwavering assistance in the field and for fruitful discussions on the sedimentology of Andros Island. Detailed and constructive reviews by Pete Burgess and Paul Enos as well as comments from Editor Brian Jones greatly improved the manuscript.

References

- Baart, F., Van Gelder, P.H., De Ronde, J., Van Koningsveld, M., Wouters, B., 2012. The effect of the 18.6-year lunar nodal cycle on regional sea-level rise estimates. *Journal of Coastal Research* 28 (2), 511–516.
- Ball, M.M., Shinn, E.A., Stockman, K.W., 1967. The geologic effects of Hurricane Donna in South Florida. *Journal of Geology* 75 (5), 583–597.
- Beach, D.K., 1995. Controls and effects of subaerial exposure on cementation and development of secondary porosity in the subsurface of Great Bahama Bank. *AAPG Memoir* 63, 1–33.
- Berkeley, A., Rankey, E.C., 2012. Progradational Holocene carbonate tidal flats of Crooked Island, south-east Bahamas: an alternative to the humid channelled belt model. *Sedimentology* 59 (6), 1902–1925.
- Beven, J., 2002. Tropical Cyclone Report: Hurricane Michelle. National Hurricane Center, Miami, FL.
- Black, M., 1932. The algal sediments of Andros Island, Bahamas. *Philosophical Transactions of the Royal Society of London. Series B, Containing Papers of a Biological Character* 222 (483–493), 165–192.
- Black, M., 1933. The precipitation of calcium carbonate on the Great Bahama Bank. *Geological Magazine* 70 (10), 455–466.
- Boss, S.K., Neumann, A.C., 1993. Impacts of Hurricane Andrew on carbonate platform environments, northern Great Bahama Bank. *Geology* 21 (10), 897–900.
- Boss, S.K., Neumann, A.C., 1995. Hurricane Andrew on Northern Great Bahama Bank: insights into storm behavior on shallow seas. *Journal of Coastal Research* 24–48.
- Budd, D.A., Hajek, E.A., Purkis, S.J., 2016. Introduction to autogenic dynamics and self-organization in sedimentary systems. *SEPM Special Publication* 106, 1–4.
- Burgess, P.M., 2001. Modeling carbonate sequence development without relative sea-level oscillations. *Geology* 29 (12), 1127–1130.
- Burgess, P.M., 2016. Identifying ordered strata: evidence, methods, and meaning. *Journal of Sedimentary Research* 86 (3), 148–167.
- Burgess, P.M., Wright, V.P., Emery, D., 2001. Numerical forward modelling of peritidal carbonate parasequence development: implications for outcrop interpretation. *Basin Research* 13 (1), 1–16.
- Davies, G.R., 1970. Carbonate Bank Sedimentation, Eastern Shark Bay, Western Australia. American Association of Petroleum Geologists (AAPG), Tulsa, Oklahoma, U.S.A., pp. 85–168.
- Demicco, R.V., Spencer, R.J., 1989. Maps—a BASIC program to model accumulation of platform sediments. *Computers and Geosciences* 15, 95–105.
- Duvat, V.K., 2019. A global assessment of atoll island planform changes over the past decades. *Wiley Interdisciplinary Reviews: Climate Change* 10 (1), 557.
- Eberli, G.P., Ginsburg, R.N., 1987. Segmentation and coalescence of Cenozoic carbonate platforms, northwestern Great Bahama Bank. *Geology* 15, 5–79.
- Fagherazzi, S., 2008. Self-organization of tidal deltas. *Proceedings of the National Academy of Sciences* 105 (48), 18692–18695.
- Fagherazzi, S., Carnielo, L., D'Alpaos, L., Defina, A., 2006. Critical bifurcation of shallow microtidal landforms in tidal flats and salt marshes. *Proceedings of the National Academy of Sciences* 103 (22), 8337–8341.
- Fischer, 1964. The Lofer cyclothems of the Alpine Triassic. In: Merriam, D.F. (Ed.), *Symposium on Cyclic Sedimentation*. Kansas State Geological Survey Bulletin, Lawrence vol. 169, pp. 107–149.
- Ford, M.R., Kench, P.S., 2015. Multi-decadal shoreline changes in response to sea level rise in the Marshall Islands. *Anthropocene* 11, 14–24.
- Gebelein, C.D., 1969. Distribution, morphology, and accretion rate of recent subtidal algal stromatolites, Bermuda. *Journal of Sedimentary Research* 39 (1), 49–69.
- Geyman, E.C., Malof, A.C., 2020. Deriving tidal structure from satellite image time series. *Earth and Space Science* 7 (2), e2019EA000958.
- Geyman, E.C., Malof, A.C., Dyer, B., 2021. How is sea level change encoded in carbonate stratigraphy? *Earth and Planetary Science Letters* 560, 116790.
- Ginsburg, R.N., 1971. Landward movement of carbonate mud: new model for regressive cycles in carbonates. *AAPG Bulletin* 55, 340 (abstract).
- Ginsburg, R.N., Hardie, L.A., 1975. Tidal and storm deposits, Northwestern Andros Island, Bahamas. In: Ginsburg, R.N. (Ed.), *Tidal Deposits*. Springer, Berlin, Heidelberg https://doi.org/10.1007/978-3-642-88494-8_23.
- Goldhammer, R.K., Lehmann, P.J., Dunn, P.A., 1993. The origin of high-frequency platform carbonate cycles and third-order sequences (Lower Ordovician El Paso Gp, West Texas): constraints from outcrop data and stratigraphic modeling. *Journal of Sedimentary Petrology* 63, 318–359.
- Hardie, L.A. (Ed.), 1977. *Sedimentation on the Modern Carbonate Tidal Flats of Northwest Andros Island, Bahamas*. Johns Hopkins University Press, Baltimore, p. 202.
- Hardie, L.A., Ginsburg, R.N., 1977. Layering: the origin and environmental significance of lamination and thin bedding. In: Hardie, L.A. (Ed.), *Sedimentation on the Modern Carbonate Tidal Flats of Northwest Andros Island, Bahamas*. Johns Hopkins University Press, Baltimore, pp. 50–123.
- Harris, P.M., Purkis, S.J., Ellis, J., 2011. Analyzing spatial patterns in modern carbonate sand bodies from Great Bahama Bank. *Journal of Sedimentary Research* 81 (3), 185–206.
- Harris, P.M., Purkis, S.J., Ellis, J., Swart, P.K., Reijmer, J.J., 2015. Mapping bathymetry and depositional facies on Great Bahama Bank. *Sedimentology* 62 (2), 566–589.
- Hernández-Cruz, L.R., Purkis, S.J., Riegl, B.M., 2006. Documenting decadal spatial changes in seagrass and *Acropora palmata* cover by aerial photography analysis in Vieques, Puerto Rico: 1937–2000. *Bulletin of Marine Science* 79 (2), 401–414.
- Iling, L.V., Wells, A.J., 1964. Penecontemporary dolomite in the Persian Gulf. *AAPG Bulletin* 48 (4), 532–533.
- Jahnert, R.J., Collins, L.B., 2013. Controls on microbial activity and tidal flat evolution in Shark Bay, Western Australia. *Sedimentology* 60 (4), 1071–1099.
- Kench, P.S., Mann, T., 2017. Reef island evolution and dynamics: insights from the Indian and Pacific Oceans and perspectives for the Spermonde Archipelago. *Frontiers in Marine Science* 4, 145.
- Kendall, C.G.S.C., d'E. Skipwith, B., P.A., 1968. Recent algal mats of a Persian Gulf lagoon. *Journal of Sedimentary Research* 38 (4), 1040–1058.
- Kenter, J.A.M., Ginsburg, R.N., Troelstra, S.R., 2001. Sea-level-driven sedimentation patterns on the slope and margin. In: Ginsburg, R.N. (Ed.), *Subsurface Geology of a Prograding Carbonate Platform Margin, Great Bahama Bank: Results of the Bahamas Drilling Project*. SEPM Special Publication vol. 70, pp. 61–100.
- Landsea, C.W., Franklin, J.L., McAdie, C.J., Beven, J.L., Gross, J.M., Jarvinen, B.R., Pasch, R.J., Rappaport, E.N., Dunion, J.P., Dodge, P.P., 2004. A reanalysis of Hurricane Andrew's intensity. *Bulletin of the American Meteorological Society* 85 (11), 1699–1712.
- Laporte, L.F., 1967. Carbonate deposition near mean sea-level and resultant facies mosaic: Manlius Formation (Lower Devonian) of New York State. *AAPG Bulletin* 51 (1), 73–101.
- Logan, B.W., Hoffman, P., Gebelein, C.D., 1974. Algal mats, cryptalgal fabrics, and structures, Hamelin Pool, Western Australia. *AAPG Memoir* 22, 140–194.
- Major, R.P., Bebout, D.G., Harris, P.M., 1996. Recent evolution of a Bahamian ooid shoal: effects of Hurricane Andrew. *Geological Society of America Bulletin* 108 (2), 168–180.
- Malof, A.C., Grotzinger, J.P., 2012. The Holocene shallowing-upward parasequence of north-west Andros Island, Bahamas. *Sedimentology* 59 (4), 1375–1407.
- Manfrino, C.M., Ginsburg, R.N., 2001. Pliocene to Pleistocene deposition history of the upper platform margin. In: Ginsburg, R.N. (Ed.), *Subsurface Geology of a Prograding Carbonate Platform Margin, Great Bahama Bank: Results of the Bahamas Drilling Project*. SEPM Special Publication vol. 70, pp. 17–40.
- Monty, C.L., 1972. Recent algal stromatolitic deposits, Andros Island, Bahamas. Preliminary report. *Geologische Rundschau* 61 (2), 742–783.
- Perkins, R.D., Enos, P., 1968. Hurricane Betsy in the Florida-Bahama area: geologic effects and comparison with hurricane Donna. *The Journal of Geology* 76 (6), 710–717.
- Pethick, J., 2001. Coastal management and sea-level rise. *Catena* 42 (2–4), 307–322.
- Purkis, S.J., Harris, P.M., 2016. The extent and patterns of sediment filling of accommodation space on Great Bahama Bank. *Journal of Sedimentary Research* 86 (4), 294–310.
- Purkis, S.J., Gardiner, R., Johnston, M.W., Sheppard, C.R., 2016. A half-century of coastline change in Diego Garcia—the largest atoll island in the Chagos. *Geomorphology* 261, 282–298.
- Purkis, S., Cavalante, G., Rohtla, L., Oehlert, A.M., Harris, P.M., Swart, P.K., 2017a. Hydrodynamic control of whitings on Great Bahama Bank. *Geology* 45 (10), 939–942.
- Purkis, S., Rivers, J., Strohmenger, C.J., Warren, C., Yousif, R., Ramirez, L., Riegl, B., 2017b. Complex interplay between depositional and petrophysical environments in Holocene tidal carbonates (Al Ruwais, Qatar). *Sedimentology* 64 (6), 1646–1675.
- Rankey, E.C., 2002. Spatial patterns of sediment accumulation on a Holocene carbonate tidal flat, northwest Andros Island, Bahamas. *Journal of Sedimentary Research* 72 (5), 591–601.
- Rankey, E.C., Morgan, J., 2002. Quantified rates of geomorphic change on a modern carbonate tidal flat, Bahamas. *Geology* 30 (7), 583–586.
- Rankey, E.C., Enos, P., Steffen, K., Druke, D., 2004. Lack of impact of Hurricane Michelle on tidal flats, Andros Island, Bahamas: integrated remote sensing and field observations. *Journal of Sedimentary Research* 74 (5), 654–661.
- Risi, J.A., Wanless, H.R., Tedesco, L.P., Gelsanliter, S., 1995. Catastrophic sedimentation from Hurricane Andrew along the southwest Florida coast. *Journal of Coastal Research* 83–102.
- Robbins, L.L., Tao, Y., Evans, C.A., 1997. Temporal and spatial distribution of whitings on Great Bahama Bank and a new lime mud budget. *Geology* 25 (10), 947–950.
- Roehl, P.O., 1967. Stony Mountain (Ordovician) and Interlake (Silurian) facies analogs of Recent low-energy marine and subaerial carbonates, Bahamas. *AAPG Bulletin* 51 (10), 1979–2032.
- Roehl, P.O., Choquette, P.W., 1985. *Carbonate Petroleum Reservoirs*. Springer, Verlag, New York.
- Shinn, E.A., 1983. Tidal flat environment. Carbonate depositional environments. *AAPG Memoir* vol. 33 pp. 172–210.
- Shinn, E.A., Ginsburg, R.N., Lloyd, R.M., 1965. Recent supratidal dolomite from Andros Island Bahamas. In: Pray, L.C., Murray, R.C. (Eds.), *Dolomitization and Limestone Diagenesis*. Soc. Econ. Paleontologists and Mineralogists Spec. Pub vol. 13, pp. 112–123.
- Shinn, E.A., Lloyd, R.M., Ginsburg, R.N., 1969. Anatomy of a modern carbonate tidal-flat, Andros Island, Bahamas. *Journal of Sedimentary Research* 39 (3), 1202–1228.
- Shreve, R.L., 1966. Statistical law of stream numbers. *The Journal of Geology* 74 (1), 17–37.
- Stewart, S.R., 2017. National Hurricane Center Tropical Cyclone Report: Hurricane Matthew. AL14016. National Oceanographic and Atmospheric Administration (NOAA).
- Taylor, K.H., Purkis, S.J., 2012. Evidence for the southward migration of mud banks in Florida Bay. *Marine Geology* 311, 52–56.
- Tedesco, L.P., Wanless, H.R., Scusa, L.A., Risi, J.A., Gelsanliter, S., 1995. Impact of Hurricane Andrew on south Florida's sandy coastlines. *Journal of Coastal Research* 59–82.
- Thieler, E.R., Himmelstoss, E.A., Zichichi, J.L., Ergul, A., 2009. The Digital Shoreline Analysis System (DSSAS) Version 4.0—An ArcGIS Extension for Calculating Shoreline Change (No. 2008-1278). US Geological Survey.
- van de Vijsel, R.C., van Belzen, J., Bouma, T.J., van der Wal, D., Cusschedu, V., Purkis, S.J., Rietkerk, M., van de Koppel, J., 2020. Estuarine biofilm patterns: modern analogues for Precambrian self-organization. *Earth Surface Processes and Landforms* 45 (5), 1141–1154.

- Wanless, H.R., Tyrrell, K.M., Tedesco, L.P., Dravis, J.J., 1988. Tidal-flat sedimentation from Hurricane Kate, Caicos Platform, British West Indies. *Journal of Sedimentary Research* 58 (4), 724–738.
- Wilkinson, B.H., Drummond, C.N., Rothman, E.D., Diedrich, N.W., 1997. Stratal order in peritidal carbonate sequences. *Journal of Sedimentary Research* 67, 1068–1082.
- Wu, M., 2020. Quantifying Inter- and Supratidal Facies-Belt Migration From Vintage Aerial Photography. University of Miami, Miami, USA (Master's thesis).
- Zhang, J., Burgess, P.M., Granjeon, D., Steel, R., 2019. Can sediment supply variations create sequences? Insights from stratigraphic forward modelling. *Basin Research* 31 (2), 274–289.